Monthly Notices of the ROYAL ASTRONOMICAL SOCIETY

MNRAS **509,** 6138–6154 (2022) https://doi.org/10.1093/mnras/stab3423
Advance Access publication 2021 November 26

Large-scale atomic data calculations in Ce V – X ions for application to early kilonova emission from neutron star mergers

H. Carvajal Gallego,[1] J. C. Berengut,[2] P. Palmeri [1] and P. Quinet [1,3]★

[1] *Physique Atomique et Astrophysique, Université de Mons, B-7000 Mons, Belgium*
[2] *School of Physics, University of New South Wales, Sydney NSW 2052, Australia*
[3] *IPNAS, Université de Liège, Sart Tilman, B-4000 Liège, Belgium*

Accepted 2021 November 19. in original form 2021 November 2

ABSTRACT

New radiative parameters (wavelengths, transition probabilities, and oscillator strengths) are reported in the present paper for a large number of spectral lines in moderately charged cerium ions, from Ce V to Ce X. These results were obtained through large-scale atomic structure calculations carried out using three different and independent theoretical approaches, namely the relativistic Hartree–Fock method, including core-polarization corrections (HFR + CPOL), the multiconfiguration Dirac–Hartree–Fock method, and the Particle-Hole Configuration Interaction (PH-CI) method implemented in the AMBiT code. The accuracy of the results was assessed through detailed comparisons between the data deduced from these methods and with the few theoretical and experimental data previously published. For the six cerium ions considered, the most complete and reliable sets of transition wavelengths and rates were then used to calculate the expansion opacities characterizing the early phases of kilonovae following neutron star mergers, i.e. for typical conditions corresponding to temperatures $T > 20\,000$ K, a density $\rho = 10^{-10}$ g cm^{-3} and a time after the merger $t = 0.1$ d.

Key words: physical data and processes – atomic data – opacity – neutron star mergers.

1 INTRODUCTION

On August 17, 2017, the interferometers *LIGO* and *VIRGO* detected for the first time the gravitational waves generated by the coalescence of two neutron stars (Abbott et al. 2017a). This event, named GW170817, was followed, 1.7 s later, by the observation of a short gamma-ray burst in the same direction by the space telescopes *FERMI* and *INTEGRAL* (Abbott et al. 2017b). This collision provoked a gigantic and very luminous explosion called kilonova, ejecting the residues in the surrounding space, whose spectral analysis by several tens of telescopes, operating in the infrared, the visible, the ultraviolet, and the X-rays, revealed the presence of heavy elements (Kasen et al. 2017).

Among the important characteristics highlighted when investigating the kilonova spectra, we will point out here the fact that the ejected material has a very high opacity. This is essentially due to the superposition of millions of spectral lines belonging to the ions of the lanthanide group ($Z = 57$–71) whose atomic structures are governed by the progressive filling of the 4f subshell giving rise to complex electronic configurations with a large amount of very close energy levels (Tanaka et al. 2018). Unfortunately, the atomic data for these elements are still too incomplete, both in quantity and quality, to model the kilonova spectra in an accurate way, especially concerning the opacity and the light curve, i.e. the evolution of the luminosity as a function of time.

Following the detection of the neutron star merger GW170817, different studies were undertaken to analyse the light emitted by the kilonova. More precisely, large-scale atomic calculations were carried out in order to model the atomic structures and radiative processes characterizing heavy ions, in particular those belonging to the lanthanide group. For this purpose, the purely relativistic theoretical methods Multiconfiguration Dirac–Hartree–Fock (MCDHF; Grant 2007, Froese Fischer et al. 2016) and Hebrew University Lawrence Livermore Atomic Code (HULLAC; Bar Shalom, Klapisch & Oreg 2001) were implemented to obtain a very large number of new fundamental parameters related to the spectral lines belonging to lanthanide atoms in their lowest ionization degrees, namely for Nd II - IV ($Z = 60$; Gaigalas et al. 2019), Er III ($Z = 68$; Gaigalas et al. 2020), the ions between Pr II ($Z = 59$) and Gd II ($Z = 64$) (Radziuté et al. 2020) and the ions between La I - IV ($Z = 57$) and Lu I - IV ($Z = 71$; Tanaka et al. 2020). In these works, the opacities due to the considered ions were also estimated, allowing to build a synthetic spectrum for the kilonova in the temperature range 0–20 000 K. The MCDHF method was also used in a detailed way for the calculation of radiative parameters and opacities in the case of Ce II - IV ions ($Z = 58$) in one of our recent works (Carvajal Gallego, Palmeri & Quinet 2021). In addition, let us remember that our Database on Rare-Earths At Mons University currently gathers radiative parameters for more than 72 000 spectral lines in neutral, singly-, doubly-, and triply-ionized lanthanides, as detailed in a review paper by Quinet & Palmeri (2020).

However, all the works mentioned above concern only the first ionization stages of lanthanide atoms (from neutrals up to triply ionized) and are therefore limited to the analysis of kilonovae in a temperature range typically below 20 000 K (Tanaka et al. 2020). In order to extend the modelling of this type of astrophysical object to higher temperatures, corresponding to the early phases of kilonovae, it is essential to know the spectroscopic properties of lanthanide ions

★ E-mail: Pascal.Quinet@umons.ac.be

in higher charge stages for which practically no investigation of the electronic structures and radiative processes has been carried out until now. On the other hand, to our knowledge, very few experimental data are available for moderately ionized lanthanide atoms. For example, if we are interested in the charge states between V and X, only the La V - X, Ce V - X, Pr V, Nd V, Yb V, and Lu V ions have experimentally known spectral lines and energy levels, according to the National Institute of Standard and Technology (NIST) bibliographic database (Kramida et al. 2020). This implies that, in most of these ions, the accuracy of theoretical calculations of atomic structures and radiative parameters cannot be estimated from comparisons with experimental data but only through the confrontation of results obtained using different and independent computational approaches.

The aim of the present work is to lay the foundation for a systematic study of lanthanide ions in the charge states between V and X and to apply the new atomic data obtained to opacity calculations for the emission spectra analysis of early phase kilonovae. Our first investigation concerns Ce V - X ions for which three different theoretical methods were used to model the atomic structures and radiative processes, namely the pseudo-relativistic Hartree–Fock method (HFR) including core-polarization effects (HFR + CPOL), the MCDHF method, and the Particle-Hole Configuration Interaction (PH-CI) method implemented in the AMBiT program. Based on detailed comparisons of the results obtained from large-scale calculations performed using these three approaches and from comparisons with the few previously published theoretical and experimental data, we were able to obtain a reliable set of new radiative parameters for a very large number of spectral lines in Ce V – X ions, allowing us to estimate the opacities due to these cerium ions in the context of early-phase kilonovae observed after neutron star mergers.

2 ATOMIC DATA CALCULATIONS

2.1 Relativistic Hartree–Fock + core-polarization method

The first method used for computing the energy levels and radiative parameters in Ce V – X ions was the pseudo-relativistic HFR method, originally introduced by Cowan (1981), and modified for taking CPOL effects into account giving rise to the so-called HFR + CPOL method, as described by Quinet et al. (1999, 2002) and Quinet (2017). As a reminder, in this approach, the largest part of intravalence correlation is taken into account by explicitly including a set of electronic configurations in the physical model, while core-excited configuration effects are modelled by a CPOL potential whose the one-particle (V_{P1}) and two-particle (V_{P2}) contributions can be written as :

$$V_{P1} = -\frac{1}{2}\,\alpha_d \sum_{i=1}^{n} \frac{r_i^2}{(r_i^2 + r_c^2)^3} \tag{1}$$

and

$$V_{P2} = -\alpha_d \sum_{i>j} \frac{\vec{r}_i.\vec{r}_j}{[(r_i^2 + r_c^2)(r_j^2 + r_c^2)]^{3/2}} \tag{2}$$

where n is the number of valence electrons, α_d is the dipole polarizability of the ionic core, and r_c is a suitable cut-off radius, which is arbitrarily chosen as a measure of the size of the ionic core.

In addition, the transition radial integral $<P_{nl} \mid r \mid P_{n'l'} >$ has also to be replaced by

$$< P_{nl}|r(1 - \frac{\alpha_d}{(r^2 + r_c^2)^{3/2}})|P_{n'l'} > \tag{3}$$

Finally, the penetration of the core by the valence electrons is taken into account by considering a further correction, as originally suggested by Hameed, Herzenberg & James (1968) and Hameed (1972), i.e. by adding the core-penetration term

$$\frac{1}{r_c^3} \int_0^{r_c} P_{nl}(r)\, r\, P_{n'l'}(r)\, \mathrm{d}r. \tag{4}$$

to the integral

$$< P_{nl}(r) \mid \frac{r}{(r^2 + r_c^2)^{3/2}} \mid P_{n'l'}(r) > \tag{5}$$

appearing in equations (2) and (3).

For each cerium ion considered in the present work, a large amount of configurations was included in the physical model. These configurations, listed in Table 1, were chosen so that the most important valence–valence (VV) correlations outside the $4d^{10}$ subshell were considered. This gave rise to a large number of calculated energy levels in Ce V – X ions, the details of which are given in Table 2. The CPOL corrections were estimated using parameters corresponding to a Pd-like Ce XIII ionic core, i.e. $\alpha_d = 0.40\ a_0^3$, and $r_c = 0.74\ a_0$. Since there are no data available in the literature for the former parameter, it was obtained by extrapolating the dipole polarizabilities published by Fraga, Karwowski & Saxena (1976) for the first ions belonging to the Pd isoelectronic sequence, from Pd I to La XII. This extrapolation is illustrated in Fig. 1. For the latter parameter, r_c, we used the average value $<r>$ corresponding to the outermost core orbital (4d), as obtained in our HFR calculations.

A first evaluation of the accuracy of the atomic structures obtained with the HFR + CPOL method could be made by observing the good overall agreement (within a few per cent) between the calculated wavelengths and those measured in laboratory. Indeed, it was found that the average relative difference $\Delta\lambda/\lambda_{Obs}$ (with $\Delta\lambda = \lambda_{HFR+CPOL} - \lambda_{Obs}$) was equal to 0.028 ± 0.081 (Ce V), −0.063 ± 0.023 (Ce VI), −0.044 + ± 0.019 (Ce VII), −0.034 ± 0.045 (Ce VIII), and −0.011 ± 0.015 (Ce X) when considering the experimental wavelengths published by Churilov et al. (2000), Joshi, Ryabtsev & Churilov (2001), Tauheed & Joshi (2008), Wajid & Jabeen (2019a, 2019b) and Wajid, Tauheed & Jabeen (2021), no experimental data being available for Ce IX to our knowledge. It is however interesting to note that the largest differences (about 25 per cent) were obtained for a few Ce V lines between 507 and 537 Å, all of them concerning $4f5s^25p^5 - 4f5s5p^6$ transitions for which we found it very complicated to theoretically reproduce the observed wavelengths mainly due to the fact that both configurations involved in the transitions appeared to be strongly perturbed by other configurations, such as $5s^25p^6$, $5s^25p^44f^2$, $5s^25p^45d^2$, $5s5p^65d$, $5s5p^54f5d$, $5p^54f^3$ for the lower even-parity one, and $5s^25p^55d$, $5s^25p^44f5d$, $5s5p^54f^2$, $5p^54f^25d$, $5p^64f5d$ for the upper odd-parity one. The full comparison between HFR + CPOL and available experimental wavelengths is shown in Fig. 2 for all the cerium ions considered in the present work.

In order to further assess the accuracy of the HFR + CPOL results, we also used two other independent theoretical approaches, namely the purely relativistic MCDHF and the PH-CI methods. More precisely, these methods were used for calculating the atomic structures and radiative parameters in three specific cerium ions (Ce V, Ce VIII, and Ce X) by developing the computational strategies described in the following two subsections.

2.2 Multiconfiguration Dirac–Hartree–Fock method

The MCDHF method described by Grant (2007) and Froese Fischer et al. (2016) was used with the latest version of General Relativistic Atomic Structure Program (GRASP), i.e. GRASP2018 (Froese

Table 1. Configurations included in the HFR + CPOL calculations for Ce V – X ions.

Ce V	Ce VI	Ce VII	Ce VIII	Ce IX	Ce X
Even parity	Odd parity	Even parity	Odd parity	Even parity	Odd parity
$5s^25p^6$	$5s^25p^5$	$5s^25p^4$	$5s^25p^3$	$5s^25p^2$	$5s^25p$
$5s^25p^56p$	$5s^25p^46p$	$5s^25p^36p$	$5s^25p^26p$	$5s^25p6p$	$5s^26p$
$5s^25p^57p$	$5s^25p^47p$	$5s^25p^37p$	$5s^25p^27p$	$5s^25p7p$	$5s^27p$
$5s^25p^58p$	$5s^25p^48p$	$5s^25p^38p$	$5s^25p^28p$	$5s^25p8p$	$5s^28p$
$5s^25p^54f$	$5s^25p^44f$	$5s^25p^34f$	$5s^25p^24f$	$5s^25p4f$	$5s^24f$
$5s^25p^55f$	$5s^25p^45f$	$5s^25p^35f$	$5s^25p^25f$	$5s^25p5f$	$5s^25f$
$5s^25p^56f$	$5s^25p^46f$	$5s^25p^36f$	$5s^25p^26f$	$5s^25p6f$	$5s^26f$
$5s^25p^57f$	$5s^25p^47f$	$5s^25p^37f$	$5s^25p^27f$	$5s^25p7f$	$5s^27f$
$5s^25p^58f$	$5s^25p^48f$	$5s^25p^38f$	$5s^25p^28f$	$5s^25p8f$	$5s^28f$
$5s^25p^44f^2$	$5s^25p^34f^2$	$5s^25p^24f^2$	$5s^25p4f^2$	$5s^24f^2$	5s5p5d
$5s^25p^45d^2$	$5s^25p^35d^2$	$5s^25p^25d^2$	$5s^25p5d^2$	$5s^25d^2$	5s5p6d
$5s^25p^46s^2$	$5s^25p^36s^2$	$5s^25p^26s^2$	$5s^25p6s^2$	$5s^26s^2$	5s5p7d
$5s^25p^45d6s$	$5s^25p^35d6s$	$5s^25p^25d6s$	$5s^25p5d6s$	$5s^25d6s$	5s5p8d
$5s5p^65d$	$5s5p^55d$	$5s5p^45d$	$5s5p^35d$	$5s5p^25d$	5s5p6s
$5s5p^66d$	$5s5p^56d$	$5s5p^46d$	$5s5p^36d$	$5s5p^26d$	5s5p7s
$5s5p^67d$	$5s5p^57d$	$5s5p^47d$	$5s5p^37d$	$5s5p^27d$	5s5p8s
$5s5p^68d$	$5s5p^58d$	$5s5p^48d$	$5s5p^38d$	$5s5p^28d$	5s4f5d
$5s5p^66s$	$5s5p^56s$	$5s5p^46s$	$5s5p^36s$	$5s5p^26s$	5s4f6d
$5s5p^67s$	$5s5p^57s$	$5s5p^47s$	$5s5p^37s$	$5s5p^27s$	5s4f7d
$5s5p^68s$	$5s5p^58s$	$5s5p^48s$	$5s5p^38s$	$5s5p^28s$	5s4f8d
$5s5p^54f5d$	$5s5p^44f5d$	$5s5p^34f5d$	$5s5p^24f5d$	5s5p4f5d	5s4f6s
$5s5p^54f6d$	$5s5p^44f6d$	$5s5p^34f6d$	$5s5p^24f6d$	5s5p4f6d	5s4f7s
$5s5p^54f7d$	$5s5p^44f7d$	$5s5p^34f7d$	$5s5p^24f7d$	5s5p4f7d	5s4f8s
$5s5p^54f8d$	$5s5p^44f8d$	$5s5p^34f8d$	$5s5p^24f8d$	5s5p4f8d	$5p^3$
$5s5p^54f6s$	$5s5p^44f6s$	$5s5p^34f6s$	$5s5p^24f6s$	5s5p4f6s	$4f^3$
$5s5p^54f7s$	$5s5p^44f7s$	$5s5p^34f7s$	$5s5p^24f7s$	5s5p4f7s	$5p4f^2$
$5s5p^54f8s$	$5s5p^44f8s$	$5s5p^34f8s$	$5s5p^24f8s$	5s5p4f8s	$5p^24f$
$5p^54f^3$	$5p^44f^3$	$5p^6$	$5p^5$	$5p^4$	
$5p^64f^2$	$5p^54f^2$	$5p^44f^2$	$5p^24f^3$	$5p4f^3$	
	$5p^64f$	$5p^54f$	$5p^34f^2$	$5p^24f^2$	
			$5p^44f$	$5p^34f$	
Odd parity	Even parity	Odd parity	Even parity	Odd parity	Even parity
$5s^25p^56s$	$5s^25p^46s$	$5s^25p^36s$	$5s^25p^26s$	$5s^25p6s$	$5s^26s$
$5s^25p^57s$	$5s^25p^47s$	$5s^25p^37s$	$5s^25p^27s$	$5s^25p7s$	$5s^27s$
$5s^25p^58s$	$5s^25p^48s$	$5s^25p^38s$	$5s^25p^38s$	$5s^25p8s$	$5s^28s$
$5s^25p^55d$	$5s^25p^45d$	$5s^25p^35d$	$5s^25p^25d$	$5s^25p5d$	$5s^25d$
$5s^25p^56d$	$5s^25p^46d$	$5s^25p^36d$	$5s^25p^26d$	$5s^25p6d$	$5s^26d$
$5s^25p^57d$	$5s^25p^47d$	$5s^25p^37d$	$5s^25p^27d$	$5s^25p7d$	$5s^27d$
$5s^25p^58d$	$5s^25p^48d$	$5s^25p^38d$	$5s^25p^28d$	$5s^25p8d$	$5s^28d$
$5s^25p^55g$	$5s^25p^45g$	$5s^25p^35g$	$5s^25p^25g$	$5s^25p5g$	$5s^25g$
$5s^25p^56g$	$5s^25p^46g$	$5s^25p^36g$	$5s^25p^26g$	$5s^25p6g$	$5s^26g$
$5s^25p^57g$	$5s^25p^47g$	$5s^25p^37g$	$5s^25p^27g$	$5s^25p7g$	$5s^27g$
$5s^25p^58g$	$5s^25p^48g$	$5s^25p^38g$	$5s^25p^28g$	$5s^25p8g$	$5s^28g$
$5s^25p^44f5d$	$5s^25p^34f5d$	$5s^25p^24f5d$	$5s^25p4f5d$	$5s^24f5d$	$5s5p^2$
$5s^25p^44f6s$	$5s^25p^34f6s$	$5s^25p^24f6s$	$5s^25p4f6s$	$5s^24f6s$	5s5p6p
$5s5p^66p$	$5s5p^6$	$5s5p^5$	$5s5p^4$	$5s5p^3$	5s5p7p
$5s5p^67p$	$5s5p^56p$	$5s5p^46p$	$5s5p^36p$	$5s5p^26p$	5s5p8p
$5s5p^68p$	$5s5p^57p$	$5s5p^47p$	$5s5p^37p$	$5s5p^27p$	5s5p4f
$5s5p^64f$	$5s5p^58p$	$5s5p^48p$	$5s5p^38p$	$5s5p^28p$	5s5p5f
$5s5p^65f$	$5s5p^54f$	$5s5p^44f$	$5s5p^34f$	$5s5p^24f$	5s5p6f
$5s5p^66f$	$5s5p^55f$	$5s5p^45f$	$5s5p^35f$	$5s5p^25f$	5s5p7f
$5s5p^67f$	$5s5p^56f$	$5s5p^46f$	$5s5p^36f$	$5s5p^26f$	5s5p8f
$5s5p^68f$	$5s5p^57f$	$5s5p^47f$	$5s5p^37f$	$5s5p^27f$	$5s4f^2$
$5s5p^54f^2$	$5s5p^58f$	$5s5p^48f$	$5s5p^38f$	$5s5p^28f$	5s4f6p
$5s5p^54f6p$	$5s5p^44f^2$	$5s5p^34f^2$	$5s5p^24f^2$	$5s5p4f^2$	5s4f7p
$5s5p^54f7p$	$5s5p^44f6p$	$5s5p^34f6p$	$5s5p^24f6p$	5s5p4f6p	5s4f8p
$5s5p^54f8p$	$5s5p^44f7p$	$5s5p^34f7p$	$5s5p^24f7p$	5s5p4f7p	$5p^25d$
$5p^54f^25d$	$5s5p^44f8p$	$5s5p^34f8p$	$5s5p^24f8p$	5s5p4f8p	$4f^25d$
$5p^64f5d$	$5p^65d$	$5p^55d$	$5p^45d$	$5p^35d$	5p4f5d
	$5p^44f^25d$	$5p^44f5d$	$5p^24f^25d$	$5p4f^25d$	
	$5p^54f5d$		$5p^34f5d$	$5p^24f5d$	

Table 2. Number of levels obtained in HFR + CPOL calculations for Ce V – X ions.

Ion	First parity[a]	Second parity[a]	Total
Ce V	1758 (e)	1686 (o)	3444
Ce VI	3941 (o)	3869 (e)	7810
Ce VII	4466 (e)	3228 (o)	7694
Ce VIII	4068 (o)	4224 (e)	8292
Ce IX	1899 (e)	2072 (o)	3971
Ce X	456 (o)	548 (e)	1001

[a](e) and (o) stand for even and odd parities, respectively.

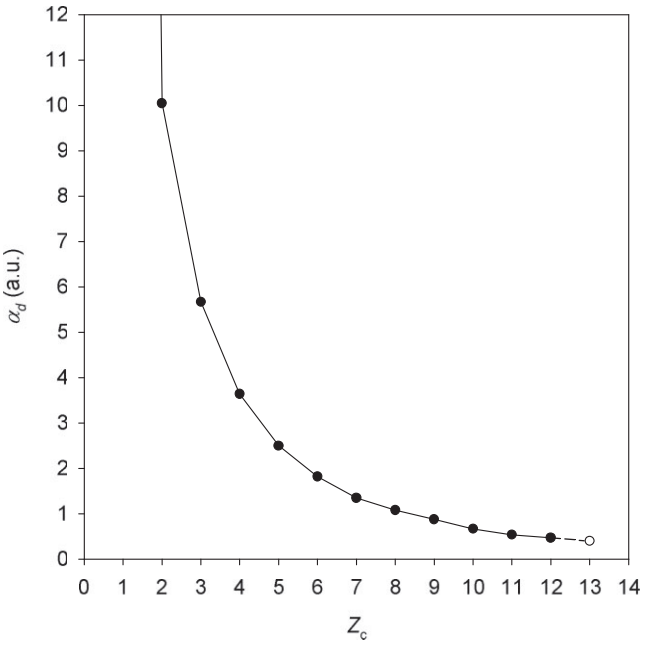

Figure 1. Static dipole polarizability, α_d, in atomic units (a_0^3) versus the ionic charge, Z_c, along the palladium isoelectronic sequence. Filled circles denote values tabulated in Fraga et al. (1976), and the open circle is the extrapolated value for Ce XIII.

Fischer, Gaigalas & Jönsson 2019). In this approach, the atomic state functions, Ψ, are represented by a superposition of configuration state functions (CSFs), Φ, with the same parity, P, total angular momentum, and total magnetic quantum numbers, J and M:

$$\psi(\gamma P J M) = \sum_{j=1}^{N_{CSF}} c_j \Phi(\gamma_j P J M), \tag{6}$$

where the label γ_j represents all the other quantum numbers needed to univoquely specify CSFs that are *jj*-coupled Slater determinants built from one-electron spin-orbitals. The configuration mixing coefficients c_j are obtained through the diagonalization of the Dirac-Coulomb Hamiltonian

$$\hat{\mathcal{H}}_{DC} = \sum_{i=1}^{N} (c\alpha.p_i + (\beta - 1)c^2 + V(r_i)) + \sum_{i>j}^{N} \frac{1}{r_{ij}}, \tag{7}$$

where $V(r)$ is the monopole part of the electron–nucleus interaction.

It should also be noted that high-order relativistic effects, i.e. the Breit interaction, QED self-energy, and vacuum polarization effects are incorporated in the relativistic configuration interaction step of the GRASP2018 package. As already mentioned above, the MCDHF method was used to compute the atomic structures and radiative parameters in Ce V, Ce VIII, and Ce X. For each of these ions, VV and core–valence (CV) correlations were included step by step from a list of configurations, constituting the so-called multireference (MR), among which all electric dipole transitions were calculated.

In the case of Ce V, the MR was chosen to include the $5s^25p^6$, $5s^25p^54f$, $5s^25p^44f^2$, $5s5p^65d$, $5p^64f^2$ even- and the $5s5p^64f$, $5s^25p^55d$, $5s5p^54f^2$ odd-parity configurations. The orbitals 1s to 5p were optimized on the $5s^25p^6$ ground configuration while the 4f and 5d orbitals were optimized using the MR configurations, keeping all other orbitals fixed. A first VV model (VV1) was built by adding to the MR configurations, single and double (SD) excitations from 5s, 5p, 5d and 4f to 5s, 5p, 5d, 5f, and 5g active orbitals. In this step, only the new orbitals, 5f and 5g, were optimized, the other ones being kept to their values obtained before. The same strategy was used to build a more elaborate VV model (VV2) by considering the additional set of 6s, 6p, 6d, 6f, and 5g active orbitals. From the latter calculation, a CV model was then built by adding SD excitations from the 4d core orbital to the MR valence orbitals, namely 5s, 5p, 5d, and 4f. This gave rise to a total of 862 213 and 675 385 J-dependent CSFs, $\Phi(\gamma PJ)$, for the even and odd parities, respectively.

For Ce VIII, the MR consisted in the $5s^25p^3$, $5s^25p^24f$, $5s^25p4f^2$, $5p^5$, $5s5p^35d$, $5p^44f$ odd configurations and the $5s5p^4$, $5s5p^34f$, $5s^25p^25d$, $5s5p^24f^2$ even configurations. VV and CV models were then built using exactly the same strategy as the one followed in the case of Ce V when considering VV1, VV2, and CV computations, the latter model leading to the consideration of 328 029 and 716 638 CSFs, $\Phi(\gamma PJ)$, in the calculations within the odd and even parities, respectively.

Finally, for Ce X, the $5s^25p$, $5s^24f$, $5s5p5d$, $5p^24f$, $5p4f^2$, $5p^3$ odd-parity configurations and the $5s5p^2$, $5s5p4f$, $5s^25d$, $5s4f^2$ even-parity configurations were considered to build the MR from which the above mentioned VV1 and VV2 models were complemented by an additional VV3 model in which the active set also included 7s, 7p, 7d, 6f, and 5g orbitals. From this latter VV3 model, CV calculations were then carried out by allowing SD excitations from the 4d core orbital to 5s, 5p, 5d, 4f, 5f, and 5g, giving rise to 849 798 and 372 663 CSFs in the odd and even parities, respectively.

A comparison of our MCDHF energy level values obtained in CV models with available experimental energy levels revealed a good agreement, the mean deviation $|\Delta E|/E_{Exp}$ being found to be equal to 0.059 ± 0.049 (Ce V), 0.000 ± 0.009 (Ce VIII), and 0.001 ± 0.015 (Ce X) when considering the experimental data reported by Wajid et al. (2021), Wajid & Jabeen (2019a), and Joshi et al. (2001), repectively.

2.3 Particle-hole configuration interaction method

The PH-CI method (Berengut 2016) as implemented in the AMBiT atomic structure code (Kahl & Berengut 2019) was the third theoretical approach used in our work to calculate the level energies and radiative parameters in three representative cerium ions, Ce V, Ce VIII, and Ce X. It consists in solving the following secular equation in matrix form (atomic units are used throughout, *i.e.* $\hbar = m_e = |e| = 1$):

$$\sum_{J \in \mathcal{P}} \left\langle I \left| \hat{\mathcal{P}} \hat{\mathcal{H}} \hat{\mathcal{P}} \right| J \right\rangle C_J = E\, C_I \tag{8}$$

where

$$\hat{\mathcal{P}} \hat{\mathcal{H}} \hat{\mathcal{P}} = \sum_i c\, \alpha \cdot p_i + (\beta - 1)\, c^2 + e_i V^{N_{\rm core}}(r_i) + \sum_{i>j} \frac{e_i\, e_j}{|r_i - r_j|} \tag{9}$$

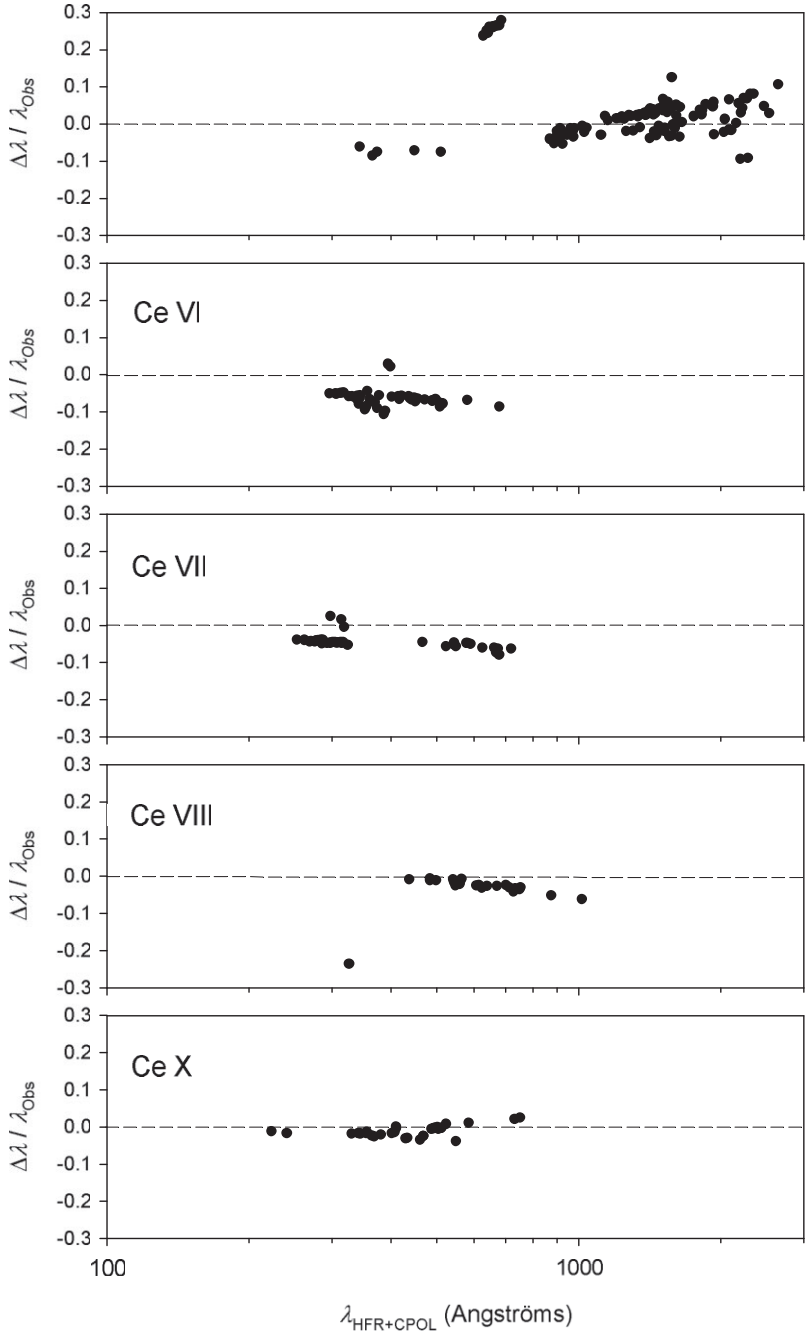

Figure 2. Deviation between HFR + CPOL and observed wavelengths, $\Delta\lambda/\lambda_{Obs}$ (with $\Delta\lambda = \lambda_{HFR+CPOL} - \lambda_{Obs}$) as a function of $\lambda_{HFR+CPOL}$ for spectral lines in Ce V, Ce VI, Ce VII, Ce VIII, and Ce X ions.

is the exact Hamiltonian operator projected on the CI space $\mathcal{P}$. The projector operator $\hat{\mathcal{P}}$ is defined as

$$\hat{\mathcal{P}}|\Psi\rangle = \sum_{I\in\mathcal{P}} |I\rangle\langle I|\Psi\rangle = \sum_{I\in\mathcal{P}} |I\rangle C_I \tag{10}$$

where $|\Psi\rangle$ is the exact total multi-electron wavefunction of the system, $\{|I\rangle \in \mathcal{P}\}$ is a complete orthonormalized basis set of multi-electron wavefunctions belonging to $\mathcal{P}$ and $C_I = \langle I|\Psi\rangle$.

The summations in equation (9) run over the valence electrons and core holes where e_i takes the values -1 for electrons and $+1$ for core holes. The potential $V^{N_{\rm core}}(r)$ includes the central-field potential generated by the $N_{\rm core}$ core electrons as felt by a valence electron or a core hole and the nuclear–electron/hole interaction potential.

The basis wavefunctions $|I\rangle$, eigen vectors of the squared total kinetic moment operator $\hat{J}^2$, and of the total parity operator $\hat{\Pi}$, are superpositions of Slater determinants built on monoelectronic spin-orbitals $|m\rangle$. The latter are obtained by solving the set of self-consistent DHF equations for the $N_{\rm core}$ core electrons,

$$\hat{h}^{\rm DHF}\,|m\rangle = \varepsilon_m\,|m\rangle \tag{11}$$

where

$$\hat{h}^{\rm DHF} = c\,\boldsymbol{\alpha}\cdot p + (\beta - 1)\,c^2 - V^{N_{\rm core}}(r). \tag{12}$$

For the valence electrons, equation (11) are solved in the frozen core potential $V^{N_{\rm core}}(r)$ of the $N_{\rm core}$ core electrons using B-spline expansions. The Breit and QED (Uehling vacuum polarization potential and self-energy) interaction terms can also be added to the DHF Hamiltonian $\hat{h}^{\rm DHF}$.

In this study, the emu CI approximation (Geddes et al. 2018) as implemented in the AMBiT code has been further used in order to reduce the size of the problem without losing much accuracy. In this approach, the set of N CI basis wavefunctions $|I\rangle$ is suitably partitioned in two subsets as follows: $N_{\rm small}$ wavefunctions $|I^{(0)}\rangle$ and $N - N_{\rm small}$ wavefunctions $|I^{(1)}\rangle$ where we impose

$$\left\langle I^{(1)} \left| \hat{\mathcal{P}}\hat{\mathcal{H}}\hat{\mathcal{P}} \right| J^{(1)} \right\rangle = 0 \ \forall \left| I^{(1)} \right\rangle \neq \left| J^{(1)} \right\rangle \tag{13}$$

as $N_{\rm small}$ important interacting basis functions $|I^{(0)}\rangle$ are considered in the zero order of perturbation theory and interact with the other $N - N_{\rm small}$ basis functions $|I^{(1)}\rangle$ in the first order.

Our AMBiT calculations have been focused on the properties of the experimental energy levels found in the literature, i.e. 51 levels of Ce V belonging to the configurations $5p^6$, $5p^5 4f$, $5p^5 5d$, $5p^5 6s$, $5p^5 6p$, and $5p^5 6d$ with symmetries $J^\Pi = 0^{\rm even} - 5^{\rm even}$, $0^{\rm odd} - 4^{\rm odd}$ published by Wajid et al. (2021), 12 levels of Ce VIII reported by Wajid & Jabeen (2019a) and belonging to the configurations $5s^2 5p^3$ and $5s5p^4$ with symmetries $J^\Pi = 1/2^{\rm even} - 5/2^{\rm even}$, $1/2^{\rm odd} - 5/2^{\rm odd}$, and 25 levels of Ce X determined by Joshi et al. (2001) and belonging to the configurations $5s^2 5p$, $5s^2 4f$, $5s^2 5d$, $5s^2 6s$, $5s5p^2$, $5s5p4f$, and $5s5p5d$ with symmetries $J^\Pi = 1/2^{\rm even} - 9/2^{\rm even}$, $1/2^{\rm odd} - 7/2^{\rm odd}$.

In order to do that, different computation strategies have been employed for the three ions. In Ce V, a model similar to the one used in Ne-like Fe XVI (Kühn et al. 2020) has been followed. In particular, the core spin-orbitals and the frozen core potential $V^{N_{\rm core}}(r)$ have been generated by solving the DHF equations for the Xe-like ground configurations $[{\rm Pd}]5s^2 5p^6$ consisting in 54 electrons. The Breit and QED interactions have been included. The valence orbitals have been determined by diagonalizing a set of B-splines using the DHF Hamiltonian with the abovementioned frozen core potential. The emu CI expansions with symmetries $J^\Pi = 0^{\rm even} - 5^{\rm even}$, $0^{\rm odd} - 4^{\rm odd}$ have been obtained by considering for the large side the SD electron and hole excitations from leading configurations $5p^6$, $5p^{-1}4f$, $5p^{-1}5d$, $5p^{-1}6s$, $5p^{-1}6p$, $5p^{-1}6d$ to the active set of orbitals 10spdfg with all the core orbitals lower than 5s inactive, i.e. 5s to 10s, 5p to 10p, 5d to 10d, 4f to 10f, and 5g to 10g. For the small side, the active set of orbitals were reduced to 6spdfg, SD electron only excitations have been considered and the leading configurations set were extended by adding $5p^{-2}4f^2$, $5s^{-1}5p^{-1}4f^2$, $5s^{-2}4f^2$, $5p^{-2}4f5d$, $5s^{-1}5p^{-1}4f5d$, and $5s^{-2}4f5d$. The resulting emu CI matrix dimensions were $N =$ 6651 739 for the large side and $N_{\rm small} =$ 13 819 for the small side. The agreements with the experimental energy levels published by Wajid et al. (2021) range from less than 1 per cent to 2 per cent except for the $5p^{-1}4f$ even levels where they clustered around 8 per cent.

Concerning Ce VIII, the DHF equations have been solved in a first step for the ground configuration of the Cd-like Ce XI system, i.e. $[{\rm Pd}]5s^2$, with 48 electrons in order to obtain the core orbitals. This enabled us to build in a second step the core electron potential $V^{N_{\rm core}}(r)$ and to solve the frozen core DHF equations for the valence orbitals. In both steps, the Breit and QED corrections have been included. In the emu CI step, the 51-electron wavefunction expansions with symmetries $J^\Pi = 1/2^{\rm even} - 5/2^{\rm even}$, $1/2^{\rm odd} - 5/2^{\rm odd}$ have been generated by considering for the large side all the SD electron and hole excitations from the $5p^3$ and $5s^{-1}5p^4$ leading configurations to the 22spdfg active set keeping all the core orbitals lower than 5s inactive. For the small side, the double electron and hole excitons have been restricted to the 12spdfg active set. The corresponding dimensions were $N =$ 1146 875 for the large side and $N_{\rm small} =$ 513 545 for the small side. The differences between our eigenvalues and the available experimental energy levels (Wajid & Jabeen 2019a) ranged from less than 1 per cent up to 2.4 per cent.

Finally, for Ce X, the strategy was similar to the one adopted for Ce VIII with the exceptions of the leading configurations and the multi-electron wavefunction symmetries. These were, respectively, 5p, $5s^{-1}5p^2$, and 4f, and $J^\Pi = 1/2^{\rm even} - 9/2^{\rm even}$, $1/2^{\rm odd} - 7/2^{\rm odd}$. The emu CI large and small side dimensions were $N =$ 577 246 and $N_{\rm small} =$ 53 973. The accords with the experimental level energies of Joshi et al. (2001) ranged from less than 1 per cent up to 5 per cent except for the 4f $^2{\rm F}^0_{5/2,7/2}$ doublet where it was about 19 per cent.

In each ion, the E1 line strengths, S, have been calculated in the Babushkin gauge with photon frequencies $\omega = 0$ (i.e. in the non-relativistic limit) using our AMBiT models for the observed transitions reported by Wajid et al. (2021), Wajid & Jabeen (2019a), and Joshi et al. (2001). The corresponding weighted oscillator strengths, gf, have been determined afterward from the AMBiT S-values using the formula given by (Cowan 1981):

$$gf \ = \ 3.0376 \times 10^{-6} \, \sigma \, S \tag{14}$$

where σ is the wavenumber in cm^{-1} of the E1 transition as deduced from the AMBiT eigenvalues and S is in au.

3 RADIATIVE PARAMETERS

Since we were able to calculate the largest number of radiative transitions with the HFR + CPOL method, which is a key element for opacity calculations, we chose the results obtained with this method as a reference set with respect to the decay rate parameters related to spectral lines in Ce V – X ions. Therefore, the weighted transition probabilities (gA) and oscillator strengths (log gf) obtained using this theoretical approach are given in Tables 3–7 for all experimentally observed lines in Ce V, Ce VI, Ce VII, Ce VIII, and Ce X, respectively. In the same tables, we also list previously published data when available, either for gA- and/or log gf-values. These latter data were taken from the works of Wajid et al. (2021) for Ce V, Churilov & Joshi (2000) for Ce VI, Wajid & Jabeen (2019b) for Ce VII, Wajid & Jabeen (2019a) for Ce VIII, and Joshi et al. (2001) for Ce X. The comparison between both sets of results is illustrated in Fig. 3 where the ratio $gA_{HFR+CPOL}$ / $gA_{Previous}$ is plotted as a function of $gA_{HFR+CPOL}$ for all the experimentally observed lines in cerium ions of interest. A quick examination of this figure indicates a relatively good overall agreement (within a factor of two) for a large majority of the transitions in each ion. However, on closer inspection, we notice that there is a much better agreement (of the order of 25 per cent on average with a much smaller dispersion in the discrepancies) in the case of Ce VII, Ce VIII, and Ce X ions. This can be explained by the fact that, for Ce V and Ce VI ions, our HFR + CPOL calculations were based on much more elaborate physical models than the theoretical investigations previously reported by Wajid et al. (2021) and Churilov & Joshi (2000), who included a smaller number of interacting configurations and did not consider CPOL effects in their HFR calculations. On the other hand, for Ce VII, Ce VIII, and Ce X ions, the radiative parameters respectively published by Wajid & Jabeen (2019b), Wajid and Jabeen (2019a), and Joshi et al.

Table 3. Transition probabilities (gA) and oscillator strengths (log gf) for experimentally observed lines in Ce V.

λ_{obs} (Å)[a]	Transition		gA (s^{-1})		log gf	
	Lower level	Upper level	Previous[a]	This work[b]	Previous[a]	This work[b]
365.661	$5s^25p^6\ ^1S_0$	$5s^25p^56s\ ^3P^o_1$	2.13E + 10	2.74E + 10		− 0.32
399.361	$5s^25p^6\ ^1S_0$	$5s^25p^55d\ ^1P^o_1$	2.81E + 11	2.88E + 11		0.76
404.209	$5s^25p^6\ ^1S_0$	$5s^25p^56s\ ^1P^o_1$	1.51E + 10	2.94E + 10		− 0.21
482.963	$5s^25p^6\ ^1S_0$	$5s^25p^55d\ ^3D^o_1$	9.15E + 09	6.68E + 09		− 0.70
507.683	$4f5s^25p^5\ ^3D_1$	$4f5s5p^6\ ^3F^o_2$	3.44E + 10	9.44E + 06		− 3.25
509.870	$4f5s^25p^5\ ^3D_2$	$4f5s5p^6\ ^3F^o_3$	2.97E + 10	1.22E + 07		− 3.13
513.193	$4f5s^25p^5\ ^3G_5$	$4f5s5p^6\ ^3F^o_4$	1.31E + 11	6.93E + 08		− 1.36
515.701	$4f5s^25p^5\ ^3D_2$	$4f5s5p^6\ ^3F^o_2$	1.99E + 10	2.75E + 07		− 2.77
518.645	$4f5s^25p^5\ ^3G_4$	$4f5s5p^6\ ^3F^o_3$	9.42E + 10	4.10E + 08		− 1.58
522.234	$4f5s^25p^5\ ^3D_3$	$4f5s5p^6\ ^3F^o_3$	2.32E + 10	6.90E + 07		− 2.35
522.841	$4f5s^25p^5\ ^3F_4$	$4f5s5p^6\ ^1F^o_3$	4.90E + 10	7.37E + 07		− 2.32
529.817	$4f5s^25p^5\ ^1D_2$	$4f5s5p^6\ ^1F^o_3$	3.31E + 10	2.79E + 08		− 1.73
535.649	$4f5s^25p^5\ ^3F_4$	$4f5s5p^6\ ^3F^o_4$	4.12E + 10	2.07E + 08		− 1.84
536.827	$4f5s^25p^5\ ^3G_3$	$4f5s5p^6\ ^3F^o_2$	4.02E + 10	3.28E + 08		− 1.64
552.134	$5s^25p^6\ ^1S_0$	$5s^25p^55d\ ^3P^o_1$	5.64E + 07	5.88E + 07		− 2.64
905.114	$5s^25p^55d\ ^3P^o_2$	$5s^25p^56p\ ^3P_2$	1.81E + 08	1.13E + 09		− 0.89
917.980	$5s^25p^55d\ ^3P^o_0$	$5s^25p^56p\ ^3S_1$	1.15E + 09	1.51E + 09		− 0.74
926.103	$5s^25p^55d\ ^3P^o_1$	$5s^25p^56p\ ^3D_2$	2.10E + 08	1.68E + 08		− 1.68
929.993	$5s^25p^55d\ ^3P^o_2$	$5s^25p^56p\ ^1P_1$	1.81E + 08	3.21E + 08		− 1.41
936.241	$5s^25p^54f\ ^1D_2$	$5s^25p^55d\ ^1P^o_1$	4.26E + 08	2.23E + 08		− 1.58
937.539	$5s^25p^55d\ ^3P^o_2$	$5s^25p^56p\ ^3D_3$	2.21E + 08	5.27E + 08		− 1.18
941.960	$5s^25p^55d\ ^3P^o_1$	$5s^25p^56p\ ^3S_1$	2.33E + 09	3.22E + 09		− 0.38
944.710	$5s^25p^55d\ ^3F^o_4$	$5s^25p^56p\ ^3D_3$	2.67E + 09	7.40E + 09		− 0.03
953.946	$5s^25p^55d\ ^3F^o_3$	$5s^25p^56p\ ^3D_3$	3.53E + 08	8.88E + 08		− 0.94
957.514	$5s^25p^55d\ ^3D^o_2$	$5s^25p^56p\ ^3P_1$	4.34E + 09	3.81E + 09		− 0.30
974.399	$5s^25p^55d\ ^3P^o_2$	$5s^25p^56p\ ^3D_2$	8.21E + 07	1.80E + 07		− 2.60
975.215	$5s^25p^55d\ ^3F^o_2$	$5s^25p^56p\ ^1P_1$	3.26E + 09	3.78E + 09		− 0.29
976.416	$5s^25p^55d\ ^3F^o_2$	$5s^25p^56p\ ^3D_1$	2.49E + 09	4.35E + 09		− 0.25
980.577	$5s^25p^55d\ ^1F^o_3$	$5s^25p^56p\ ^3D_2$	5.33E + 09	7.27E + 04		− 5.00
991.965	$5s^25p^55d\ ^3P^o_2$	$5s^25p^56p\ ^3S_1$	1.95E + 09	2.60E + 09		− 0.43
992.129	$5s^25p^55d\ ^3F^o_3$	$5s^25p^56p\ ^3D_2$	2.09E + 09	2.13E + 09		− 0.51
1010.827	$5s^25p^55d\ ^3D^o_3$	$5s^25p^56p\ ^3P_2$	8.07E + 08	3.33E + 09		− 0.32
1024.151	$5s^25p^55d\ ^3F^o_2$	$5s^25p^56p\ ^3D_2$	5.08E + 08	4.17E + 08		− 1.19
1043.576	$5s^25p^55d\ ^3F^o_2$	$5s^25p^56p\ ^3S_1$	9.37E + 07	5.53E + 07		− 2.06
1051.112	$5s^25p^55d\ ^3D^o_1$	$5s^25p^56p\ ^3P_0$	9.77E + 08	7.67E + 08		− 0.90
1051.438	$5s^25p^55d\ ^3D^o_3$	$5s^25p^56p\ ^3D_3$	2.07E + 08	5.26E + 08		− 1.08
1114.848	$5s^25p^56p\ ^3D_3$	$5s^25p^56d\ ^3F^o_3$	2.77E + 06	4.63E + 06		− 3.05
1141.824	$4f5s^25p^5\ ^3D_2$	$5s^25p^55d\ ^3D^o_3$	9.67E + 06	1.35E + 07		− 2.57
1150.225	$5s^25p^55d\ ^3D^o_1$	$5s^25p^56p\ ^1P_1$	6.19E + 08	6.26E + 08		− 0.93
1186.865	$4f5s^25p^5\ ^3G_4$	$5s^25p^55d\ ^3D^o_3$	2.62E + 07	4.83E + 07		− 1.98
1205.859	$4f5s^25p^5\ ^3D_3$	$5s^25p^55d\ ^3D^o_3$	1.15E + 08	1.27E + 08		− 1.54
1211.818	$4f5s^25p^5\ ^1D_2$	$5s^25p^55d\ ^3D^o_1$	2.48E + 08	2.26E + 08		− 1.29
1234.403	$4f5s^25p^5\ ^3D_2$	$5s^25p^55d\ ^3F^o_2$	1.93E + 07	2.21E + 07		− 2.28
1250.718	$4f5s^25p^5\ ^3G_3$	$5s^25p^55d\ ^3D^o_3$	5.48E + 06	8.14E + 05		− 3.70
1264.429	$4f5s^25p^5\ ^3D_1$	$5s^25p^55d\ ^3P^o_2$	9.64E + 06	1.08E + 07		− 2.57
1286.305	$4f5s^25p^5\ ^3F_3$	$5s^25p^55d\ ^1F^o_3$	5.16E + 07	3.31E + 07		− 2.10
1299.297	$4f5s^25p^5\ ^3F_4$	$5s^25p^55d\ ^1F^o_3$	5.92E + 08	7.25E + 08		− 0.72
1309.589	$4f5s^25p^5\ ^3D_3$	$5s^25p^55d\ ^3F^o_2$	1.10E + 07	7.83E + 06		− 2.68
1315.354	$4f5s^25p^5\ ^3D_2$	$5s^25p^55d\ ^3P^o_2$	1.45E + 08	1.41E + 08		− 1.41
1315.826	$4f5s^25p^5\ ^3F_4$	$5s^25p^55d\ ^3D^o_3$	5.50E + 08	6.23E + 08		− 0.77
1331.550	$4f5s^25p^5\ ^3F_3$	$5s^25p^55d\ ^3D^o_2$	4.83E + 08	3.90E + 05		− 4.00
1341.640	$4f5s^25p^5\ ^3G_4$	$5s^25p^55d\ ^3F^o_3$	3.73E + 08	5.91E + 08		− 0.77
1356.192	$4f5s^25p^5\ ^3D_1$	$5s^25p^55d\ ^3P^o_1$	9.56E + 07	9.92E + 07		− 1.54
1358.358	$4f5s^25p^5\ ^3G_3$	$5s^25p^55d\ ^3F^o_2$	3.54E + 08	4.92E + 08		− 0.84
1360.331	$4f5s^25p^5\ ^3G_4$	$5s^25p^55d\ ^3F^o_4$	4.23E + 07	4.76E + 07		− 1.85
1360.786	$4f5s^25p^5\ ^1D_2$	$5s^25p^55d\ ^3D^o_3$	1.56E + 04	3.77E + 06		− 2.96
1362.125	$4f5s^25p^5\ ^3G_5$	$5s^25p^55d\ ^3F^o_4$	4.62E + 08	8.12E + 08		− 0.61
1362.463	$5s^25p^56s\ ^3P^o_2$	$5s^25p^56p\ ^3P_1$	1.89E + 08	9.18E + 07		− 1.60
1362.668	$4f5s^25p^5\ ^3G_3$	$5s^25p^55d\ ^3F^o_2$	3.15E + 08	4.43E + 08		− 0.88
1365.964	$4f5s^25p^5\ ^3D_3$	$5s^25p^55d\ ^3F^o_3$	7.74E + 07	5.96E + 07		− 1.75
1385.346	$4f5s^25p^5\ ^3D_3$	$5s^25p^55d\ ^3F^o_4$	4.58E + 06	1.22E + 07		− 2.42
1401.064	$4f5s^25p^5\ ^3D_3$	$5s^25p^55d\ ^3P^o_2$	3.20E + 08	3.52E + 08		− 0.96
1401.241	$5s^25p^55d\ ^1P^o_1$	$5s^25p^56p\ ^1S_0$	5.14E + 08	2.05E + 08		− 1.12

Table 3 – *continued*

λ_{obs} (Å)[a]	Transition		gA (s^{-1})		log gf	
	Lower level	Upper level	Previous[a]	This work[b]	Previous[a]	This work[b]
1409.195	$4f5s^25p^5\ ^3D_1$	$5s^25p^55d\ ^3P^o_0$	9.21E + 07	9.78E + 07		− 1.51
1414.959	$4f5s^25p^5\ ^3D_2$	$5s^25p^55d\ ^3P^o_1$	1.84E + 08	1.96E + 08		− 1.21
1415.046	$5s^25p^56p\ ^3D_1$	$5s^25p^56d\ ^3D^o_1$	1.15E + 09	1.06E + 08		− 1.44
1423.824	$4f5s^25p^5\ ^3G_3$	$5s^25p^55d\ ^3F^o_3$	6.74E + 07	7.09E + 07		− 1.63
1444.901	$4f5s^25p^5\ ^3G_3$	$5s^25p^55d\ ^3F^o_4$	6.21E + 06	4.93E + 06		− 2.77
1457.288	$5s^25p^56p\ ^3D_1$	$5s^25p^56d\ ^3D^o_2$	3.79E + 07	9.92E + 06		− 2.47
1459.172	$5s^25p^56p\ ^3D_1$	$5s^25p^56d\ ^3F^o_2$	6.25E + 09	2.35E + 08		− 1.07
1473.624	$5s^25p^56p\ ^3D_2$	$5s^25p^56d\ ^1D^o_2$	1.28E + 09	9.61E + 08		− 0.54
1475.078	$5s^25p^56p\ ^3S_1$	$5s^25p^56d\ ^3P^o_2$	4.15E + 09	3.14E + 09		− 0.01
1487.498	$5s^25p^56p\ ^1P_1$	$5s^25p^56d\ ^1P^o_1$	2.34E + 09	1.38E + 09		− 0.34
1494.356	$4f5s^25p^5\ ^1D_2$	$5s^25p^55d\ ^3F^o_2$	7.33E + 07	6.49E + 07		− 1.64
1507.607	$5s^25p^56p\ ^3D_2$	$5s^25p^56d\ ^3F^o_3$	5.47E + 09	4.20E + 09		0.13
1508.812	$4f5s^25p^5\ ^3F_4$	$5s^25p^55d\ ^3F^o_3$	6.46E + 05	1.23E + 07		− 2.34
1518.101	$5s^25p^56p\ ^3S_1$	$5s^25p^56d\ ^3P^o_1$	5.10E + 09	2.87E + 09		− 0.02
1532.497	$4f5s^25p^5\ ^3F_4$	$5s^25p^55d\ ^3F^o_4$	9.51E + 07	6.87E + 07		− 1.57
1540.573	$5s^25p^56p\ ^3S_1$	$5s^25p^56d\ ^3P^o_0$	2.17E + 09	1.12E + 09		− 0.41
1549.367	$5s^25p^56p\ ^3D_3$	$5s^25p^56d\ ^3D^o_3$	7.94E + 08	8.42E + 08		− 0.54
1568.225	$4f5s^25p^5\ ^1D_2$	$5s^25p^55d\ ^3F^o_3$	5.83E + 06	8.18E + 06		− 2.48
1575.641	$4f5s^25p^5\ ^1D_2$	$5s^25p^55d\ ^3D^o_1$	5.57E + 07	8.83E + 07		− 1.46
1588.325	$5s^25p^56p\ ^1P_1$	$5s^25p^56d\ ^1D^o_2$	6.21E + 09	3.85E + 09		0.16
1599.641	$5s^25p^56p\ ^3D_2$	$5s^25p^56d\ ^3F^o_3$	9.53E + 09	2.01E + 09		− 0.11
1605.239	$5s^25p^56p\ ^3D_3$	$5s^25p^56d\ ^3F^o_3$	3.93E + 08	8.05E + 08		− 0.51
1608.160	$5s^25p^56p\ ^3D_3$	$5s^25p^56d\ ^3F^o_4$	4.48E + 09	4.66E + 09		0.26
1610.488	$5s^25p^56p\ ^1S_0$	$5s^25p^56d\ ^3D^o_1$	2.02E + 09	7.69E + 08		− 0.55
1621.270	$5s^25p^56p\ ^3P_1$	$5s^25p^56d\ ^3D^o_2$	8.77E + 09	1.72E + 09		− 0.18
1628.460	$5s^25p^56p\ ^3D_2$	$5s^25p^56d\ ^3F^o_2$	1.03E + 09	2.58E + 08		− 1.02
1646.859	$5s^25p^56p\ ^3P_2$	$5s^25p^56d\ ^3D^o_3$	1.36E + 09	2.59E + 09		0.03
1694.062	$5s^25p^56p\ ^3P_0$	$5s^25p^56d\ ^1P^o_1$	2.42E + 09	1.05E + 09		− 0.37
1720.590	$5s^25p^56p\ ^3P_2$	$5s^25p^56d\ ^3P^o_2$	3.68E + 08	1.05E + 09		− 0.31
1741.233	$4f5s^25p^5\ ^3F_3$	$5s^25p^55d\ ^3D^o_3$	4.32E + 06	4.29E + 06		− 2.68
1765.111	$4f5s^25p^5\ ^3F_4$	$5s^25p^55d\ ^3D^o_3$	4.77E + 06	8.96E + 06		− 2.35
1767.382	$4f5s^25p^5\ ^1D_2$	$5s^25p^55d\ ^3P^o_1$	1.93E + 05	5.77E + 05		− 3.52
1779.403	$5s^25p^56p\ ^3P_2$	$5s^25p^56d\ ^3P^o_1$	6.45E + 07	1.46E + 08		− 1.14
1824.990	$5s^25p^56s\ ^1P^o_1$	$5s^25p^56p\ ^3P_0$	7.85E + 08	4.57E + 08		− 0.59
1841.673	$4f5s^25p^5\ ^3G_3$	$5s^25p^55d\ ^3F^o_2$	3.65E + 05	1.80E + 04		− 5.00
1955.172	$4f5s^25p^5\ ^3G_3$	$5s^25p^55d\ ^3F^o_3$	4.31E + 06	7.67E + 05		− 3.30
1991.325	$5s^25p^56s\ ^3P^o_2$	$5s^25p^56p\ ^3P_2$	2.00E + 08	7.74E + 08		− 0.36
2018.054	$5s^25p^56s\ ^1P^o_1$	$5s^25p^56p\ ^3P_2$	2.78E + 08	4.66E + 08		− 0.53
2070.845	$5s^25p^56s\ ^3P^o_1$	$5s^25p^56p\ ^1S_0$	4.87E + 08	2.25E + 08		− 0.79
2081.251	$5s^25p^56s\ ^3P^o_0$	$5s^25p^56p\ ^3P^o_1$	1.27E + 09	4.90E + 08		− 0.52
2095.999	$4f5s^25p^5\ ^3F_3$	$5s^25p^55d\ ^3F^o_3$	4.63E + 06	2.92E + 06		− 2.66
2115.855	$5s^25p^56s\ ^3P^o_2$	$5s^25p^56p\ ^1P_1$	3.82E + 07	5.14E + 07		− 1.47
2130.691	$4f5s^25p^5\ ^3F_4$	$5s^25p^55d\ ^3F^o_3$	1.75E + 05	1.67E + 06		− 2.89
2135.022	$5s^25p^56s\ ^3P^o_1$	$5s^25p^56p\ ^3D_2$	6.57E + 06	1.36E + 09		0.00
2141.969	$4f5s^25p^5\ ^3F_3$	$5s^25p^55d\ ^3F^o_4$	6.00E + 08	5.10E + 06		− 2.39
2143.434	$5s^25p^56s\ ^3P^o_1$	$5s^25p^56p\ ^3P_1$	1.54E + 09	4.17E + 08		− 0.56
2146.057	$5s^25p^56s\ ^1P^o_1$	$5s^25p^56p\ ^1P_1$	1.12E + 09	9.90E + 08		− 0.14
2155.318	$5s^25p^56s\ ^3P^o_2$	$5s^25p^56p\ ^3D_3$	8.67E + 06	1.65E + 09		0.06
2178.222	$4f5s^25p^5\ ^3F_4$	$5s^25p^55d\ ^3F^o_4$	3.07E + 08	3.25E + 06		− 2.57
2360.591	$5s^25p^56s\ ^3P^o_2$	$5s^25p^56p\ ^3D_2$	5.02E + 08	8.47E + 07		− 1.11
2398.256	$5s^25p^56s\ ^1P^o_1$	$5s^25p^56p\ ^3D_2$	2.10E + 08	3.58E + 08		− 0.42
2432.642	$5s^25p^56s\ ^3P^o_0$	$5s^25p^56p\ ^3D_1$	1.10E + 09	5.63E + 08		− 0.39
2466.420	$5s^25p^56s\ ^3P^o_2$	$5s^25p^56p\ ^3S_1$	5.95E + 08	7.52E + 08		− 0.14
2518.038	$5s^25p^56s\ ^3P^o_1$	$5s^25p^56p\ ^3D_1$	2.13E + 10	1.96E + 08		− 0.81

[a]Wajid et al. (2021)
[b]HFR + CPOL calculations

(2001) were based on more complete theoretical approaches. Indeed, in the case of Ce VII and Ce VIII, Wajid and Jabeen used the purely relativistic MCDF method taking many VV and CV interactions into account up to $n = 8$ from the $5s^25p^4$, $5s5p^5$ and $5s^25p^3$, $5s5p^4$, $5s^25p^25d$, $5s^25p^26s$ MRs, respectively. For Ce X, although the HFR calculations performed by Joshi et al. (2001) were less extensive than ours, they still accounted for the most important VV correlation effects thanks to the inclusion of 13 odd-parity and 12 even-parity configurations in their model, this ion, with a $5s^25p$ ground configuration, having a less complex electronic structure

Table 4. Transition probabilities (gA) and oscillator strengths (log gf) for experimentally observed lines in Ce VI.

λ_{obs} (Å)[a]	Transition		gA (s^{-1})		log gf	
	Lower level	Upper level	Previous[a]	This work[b]	Previous[a]	This work[b]
311.989	$5s^25p^5\ ^2P^o_{1/2}$	$5s^25p^4(^3P)6s\ 346509_{1/2}$	9.60E + 09	1.82E + 10		− 0.62
321.678	$5s^25p^5\ ^2P^o_{3/2}$	$5s^25p^4(^3P)6s\ 310870_{3/2}$	9.90E + 09	8.81E + 09		− 0.91
323.020	$5s^25p^5\ ^2P^o_{3/2}$	$5s^25p^4(^3P)6s\ 309578_{5/2}$	5.00E + 10	5.48E + 10		− 0.11
328.952	$5s^25p^5\ ^2P^o_{3/2}$	$5s^25p^4(^3P)6s\ 303995_{1/2}$	1.95E + 10	2.64E + 10		− 0.41
332.998	$5s^25p^5\ ^2P^o_{3/2}$	$5s^25p^4(^3P)6s\ 300301_{3/2}$	2.51E + 10	2.71E + 10		− 0.39
345.313	$5s^25p^5\ ^2P^o_{3/2}$	$5s^25p^4(^3P)6s\ 288592_{1/2}$	5.50E + 09	8.05E + 09		− 0.89
351.019	$5s^25p^5\ ^2P^o_{1/2}$	$5s^25p^4(^3P)6s\ 310870_{3/2}$	4.28E + 10	4.87E + 10		− 0.10
359.699	$5s^25p^5\ ^2P^o_{1/2}$	$5s^25p^4(^3P)6s\ 303995_{1/2}$	2.53E + 10	3.23E + 10		− 0.25
361.140	$5s^25p^5\ ^2P^o_{3/2}$	$5s^25p^4(^3P)6s\ 276899_{3/2}$	6.92E + 10	8.63E + 10		0.17
364.543	$5s^25p^5\ ^2P^o_{1/2}$	$5s^25p^4(^3P)6s\ 300301_{3/2}$	1.60E + 09	6.69E + 09		− 0.92
366.323	$5s^25p^5\ ^2P^o_{3/2}$	$5s^25p^4(^3P)6s\ 272983_{5/2}$	5.60E + 09	6.46E + 09		− 0.94
370.565	$5s^25p^5\ ^2P^o_{3/2}$	$5s^25p^4(^3P)5d\ 269857_{1/2}$	2.60E + 09	1.10E + 10		− 0.71
372.816	$5s^25p^5\ ^2P^o_{3/2}$	$5s^25p^4(^3P)5d\ 268229_{5/2}$	4.00E + 08	2.70E + 11		0.71
383.440	$5s^25p^5\ ^2P^o_{1/2}$	$5s^25p^4(^3P)5d\ 286782_{3/2}$	1.88E + 11	2.73E + 08		− 2.19
385.839	$5s^25p^5\ ^2P^o_{3/2}$	$5s^25p^4(^3P)5d\ 259175_{5/2}$	6.41E + 11	2.56E + 09		− 1.30
387.312	$5s^25p^5\ ^2P^o_{3/2}$	$5s^25p^4(^3P)5d\ 258190_{3/2}$	2.46E + 11	1.83E + 11		0.54
388.784	$5s^25p^5\ ^2P^o_{3/2}$	$5s^25p^4(^3P)5d\ 257211_{1/2}$	2.24E + 11	1.82E + 11		0.53
390.048	$5s^25p^5\ ^2P^o_{1/2}$	$5s^25p^4(^3P)5d\ 282363_{3/2}$	1.86E + 11	3.01E + 08		− 2.14
398.545	$5s^25p^5\ ^2P^o_{1/2}$	$5s^25p^4(^3P)6s\ 276899_{3/2}$	4.00E + 08	1.10E + 08		− 2.64
399.448	$5s^25p^5\ ^2P^o_{3/2}$	$5s^25p^4(^3P)5d\ 250345_{3/2}$	8.64E + 10	2.18E + 10		− 0.32
410.053	$5s^25p^5\ ^2P^o_{1/2}$	$5s^25p^4(^3P)5d\ 269857_{1/2}$	1.57E + 11	1.43E + 11		0.48
426.917	$5s^25p^5\ ^2P^o_{3/2}$	$5s^25p^4(^3P)5d\ 234237_{5/2}$	6.10E + 09	3.89E + 09		− 1.03
430.653	$5s^25p^5\ ^2P^o_{1/2}$	$5s^25p^4(^3P)5d\ 258190_{3/2}$	1.37E + 10	7.73E + 08		− 1.76
432.481	$5s^25p^5\ ^2P^o_{1/2}$	$5s^25p^4(^3P)5d\ 257211_{1/2}$	6.70E + 09	1.78E + 09		− 1.40
439.717	$5s^25p^5\ ^2P^o_{3/2}$	$5s^25p^4(^3P)5d\ 227419_{5/2}$	7.00E + 08	1.99E + 09		− 1.29
444.942	$5s^25p^5\ ^2P^o_{3/2}$	$5s^25p^4(^3P)5d\ 224748_{5/2}$	9.50E + 09	2.62E + 09		− 1.16
445.713	$5s^25p^5\ ^2P^o_{1/2}$	$5s^25p^4(^3P)5d\ 250345_{3/2}$	2.50E + 10	1.32E + 10		− 0.46
446.633	$5s^25p^5\ ^2P^o_{3/2}$	$5s^25p^4(^3P)5d\ 223899_{3/2}$	1.00E + 08	2.63E + 06		− 4.00
463.376	$5s^25p^5\ ^2P^o_{3/2}$	$5s^25p^4(^3P)5d\ 215807_{3/2}$	1.40E + 09	4.94E + 08		− 1.85
467.558	$5s^25p^5\ ^2P^o_{3/2}$	$5s^25p^4(^3P)5d\ 213877_{5/2}$	4.00E + 09	3.04E + 09		− 1.06
474.178	$5s^25p^5\ ^2P^o_{3/2}$	$5s^25p^4(^3P)5d\ 210891_{3/2}$	9.30E + 09	5.64E + 09		− 0.78
475.343	$5s^25p^5\ ^2P^o_{3/2}$	$5s^25p^4(^3P)5d\ 210374_{5/2}$	1.09E + 10	4.87E + 09		− 0.84
478.387	$5s^25p^5\ ^2P^o_{3/2}$	$5s^25p^4(^3P)5d\ 209037_{1/2}$	1.00E + 08	2.00E + 09		− 1.44
485.117	$5s^25p^5\ ^2P^o_{3/2}$	$5s^25p^4(^3P)5d\ 206135_{1/2}$	8.70E + 09	2.05E + 09		− 1.21
487.679	$5s^25p^5\ ^2P^o_{3/2}$	$5s^25p^4(^3P)5d\ 205055_{3/2}$	2.20E + 09	9.96E + 08		− 1.51
505.268	$5s^25p^5\ ^2P^o_{1/2}$	$5s^25p^4(^3P)5d\ 223899_{3/2}$	4.00E + 08	1.22E + 08		− 2.40
526.234	$5s^25p^5\ ^2P^o_{3/2}$	$5s^25p^4(^3P)5d\ 190030_{1/2}$	2.00E + 08	3.80E + 07		− 2.85
526.811	$5s^25p^5\ ^2P^o_{1/2}$	$5s^25p^4(^3P)5d\ 215807_{3/2}$	2.00E + 08	2.51E + 08		− 2.06
531.723	$5s^25p^5\ ^2P^o_{3/2}$	$5s^25p^4(^3P)5d\ 188068_{3/2}$	1.00E + 08	5.88E + 07		− 2.66
533.058	$5s^25p^5\ ^2P^o_{3/2}$	$5s^25p^4(^3P)5d\ 187597_{5/2}$	2.00E + 08	1.43E + 08		− 2.27
546.288	$5s^25p^5\ ^2P^o_{1/2}$	$5s^25p^4(^3P)5d\ 209037_{1/2}$	1.00E + 08	4.04E + 07		− 2.80
555.100	$5s^25p^5\ ^2P^o_{1/2}$	$5s^25p^4(^3P)5d\ 206135_{1/2}$	5.00E + 08	7.08E + 07		− 2.57
558.436	$5s^25p^5\ ^2P^o_{1/2}$	$5s^25p^4(^3P)5d\ 205055_{3/2}$	1.00E + 08	5.60E + 07		− 2.66
623.379	$5s^25p^5\ ^2P^o_{3/2}$	$5s5p^6\ 160416_{1/2}$	2.60E + 09	1.04E + 09		− 1.28
743.876	$5s^25p^5\ ^2P^o_{1/2}$	$5s5p^6\ 160416_{1/2}$	1.20E + 09	5.50E + 08		− 1.42

[a]Churilov et al. (2000) [b]HFR + CPOL calculations

than those characterizing lower ionization stages of cerium atom. We can thus conclude that the oscillator strengths and transition probabilities determined in our work with the HFR + CPOL method show better agreement with the few most reliable results previously published.

To further estimate the accuracy of our HFR + CPOL calculations, we also compared them with the radiative parameters obtained in our work using the MCDHF and AMBiT methods for Ce V, Ce VIII, and Ce X ions. Such comparisons are reported in Table 8 for experimentally observed lines in these ions and further illustrated in Figs 4 and 5 in which our HFR + CPOL log gf-values are plotted against MCDHF and AMBiT results, respectively. Looking at this table and these two figures, it is interesting to see that the three theoretical approaches show good mutual agreement. Specifically, if we look at the HFR + CPOL gf-values for the whole set of transitions listed in Table 8, we note that they show average relative differences of about 40 per cent and 35 per cent when compared to the MCDHF and AMBiT results, respectively, these deviations being reduced to 35 per cent and 30 per cent if we consider only the most intense lines with log $gf > -2.0$.

All these considerations allow us to deduce that the HFR + CPOL radiative parameters obtained in the present work represent a reliable

Table 5. Transition probabilities (gA) and oscillator strengths (log gf) for experimentally observed lines in Ce VII.

λ_{obs} (Å)[a]	Transition		gA (s^{-1})		log gf	
	Lower level	Upper level	Previous[b]	This work[c]	Previous[b]	This work[c]
262.945	$5s^25p^4\ ^3P_2$	$5s^25p^36s\ ^1P^o_1$	3.48E + 08	4.14E + 08	− 2.46	− 2.40
273.144	$5s^25p^4\ ^3P_0$	$5s^25p^36s\ ^1P^o_1$	3.63E + 08	1.55E + 08	− 2.40	− 2.80
281.211	$5s^25p^4\ ^3P_1$	$5s^25p^36s\ ^1P^o_1$	1.38E + 09	2.98E + 09	− 1.80	− 1.49
282.720	$5s^25p^4\ ^3P_1$	$5s^25p^36s\ ^1P^o_1$	6.75E + 09	8.20E + 09	− 1.10	− 1.04
288.039	$5s^25p^4\ ^1D_2$	$5s^25p^36s\ ^1P^o_1$	1.72E + 10	2.37E + 10	− 0.68	− 0.57
289.619	$5s^25p^4\ ^1D_2$	$5s^25p^36s\ ^1P^o_2$	8.85E + 09	7.70E + 09	− 0.97	− 1.05
289.655	$5s^25p^4\ ^3P_2$	$5s^25p^36s\ ^1P^o_2$	1.09E + 10	1.39E + 10	− 0.87	− 0.79
290.291	$5s^25p^4\ ^3P_0$	$5s^25p^36s\ ^1P^o_1$	1.38E + 10	3.97E + 09	− 0.77	− 1.28
292.123	$5s^25p^4\ ^3P_2$	$5s^25p^36s\ ^1P^o_3$	3.84E + 10	8.00E + 10	− 0.32	− 0.03
295.643	$5s^25p^4\ ^3P_2$	$5s^25p^36s\ ^1P^o_1$	8.04E + 09	8.10E + 09	− 0.99	− 1.01
298.564	$5s^25p^4\ ^3P_2$	$5s^25p^36s\ ^1P^o_2$	1.77E + 10	3.74E + 10	− 0.52	− 0.34
299.416	$5s^25p^4\ ^3P_1$	$5s^25p^36s\ ^1P^o_1$	3.75E + 09	3.10E + 09	− 1.38	− 1.42
299.891	$5s^25p^4\ ^3P_1$	$5s^25p^36s\ ^1P^o_0$	5.31E + 09	6.34E + 09	− 1.16	− 1.11
307.170	$5s^25p^4\ ^1D_2$	$5s^25p^36s\ ^1P^o_1$	1.29E + 10	2.74E + 09	− 0.76	− 1.45
308.620	$5s^25p^4\ ^3P_0$	$5s^25p^36s\ ^1P^o_1$	8.64E + 08	4.56E + 09	− 1.92	− 1.17
311.984	$5s^25p^4\ ^3P_1$	$5s^25p^36s\ ^1P^o_2$	1.16E + 10	1.74E + 10	− 0.79	− 0.64
314.984	$5s^25p^4\ ^3P_2$	$5s^25p^36s\ ^1P^o_1$	5.28E + 10	9.96E + 09	− 0.12	− 0.87
318.946	$5s^25p^4\ ^3P_1$	$5s^25p^36s\ ^1P^o_1$	4.47E + 10	3.18E + 10	− 0.18	− 0.35
319.459	$5s^25p^4\ ^3P_2$	$5s^25p^36s\ ^1P^o_2$	1.27E + 09	6.07E + 09	− 1.71	− 1.04
320.412	$5s^25p^4\ ^1D_2$	$5s^25p^36s\ ^1P^o_2$	1.10E + 11	1.03E + 11	0.22	0.16
322.340	$5s^25p^4\ ^3P_1$	$5s^25p^36s\ ^1P^o_2$	3.87E + 09	8.36E + 09	− 1.23	− 0.93
323.433	$5s^25p^4\ ^1D_2$	$5s^25p^36s\ ^1P^o_3$	8.75E + 09	7.39E + 09	− 0.88	− 0.98
327.760	$5s^25p^4\ ^1D_2$	$5s^25p^36s\ ^1P^o_1$	6.48E + 09	3.30E + 09	− 0.99	− 1.31
329.744	$5s^25p^4\ ^3P_0$	$5s^25p^36s\ ^1P^o_1$	2.22E + 10	8.73E + 09	− 0.45	− 0.89
331.353	$5s^25p^4\ ^1D_2$	$5s^25p^36s\ ^1P^o_2$	7.00E + 09	4.00E + 09	− 0.95	− 1.22
341.580	$5s^25p^4\ ^3P_1$	$5s^25p^36s\ ^1P^o_1$	9.00E + 09	3.54E + 09	− 0.81	− 1.25
487.862	$5s^25p^4\ ^3P_2$	$5s^25p^35d\ ^5D^o_1$		3.29E + 08		− 1.97
554.709	$5s^25p^4\ ^3P_1$	$5s^25p^35d\ ^5D^o_1$		4.40E + 08		− 1.74
571.236	$5s^25p^4\ ^3P_2$	$5s5p^5\ ^3P^o_1$	2.87E + 09	2.43E + 09	− 0.85	− 0.97
572.450	$5s^25p^4\ ^1D_2$	$5s5p^5\ ^1P^o_1$	4.29E + 09	3.89E + 09	− 0.68	− 0.76
581.935	$5s^25p^4\ ^1D_2$	$5s^25p^35d\ ^5D^o_1$		1.60E + 09		− 1.14
606.582	$5s^25p^4\ ^3P_1$	$5s5p^5\ ^3P^o_0$	1.19E + 09	1.04E + 09	− 1.18	− 1.29
611.894	$5s^25p^4\ ^3P_2$	$5s5p^5\ ^3P^o_2$	4.20E + 09	3.53E + 09	− 0.63	− 0.75
621.703	$5s^25p^4\ ^3P_0$	$5s5p^5\ ^3P^o_1$	1.01E + 09	9.46E + 08	− 1.23	− 1.31
665.114	$5s^25p^4\ ^3P_1$	$5s5p^5\ ^3P^o_1$	7.38E + 08	6.61E + 08	− 1.32	− 1.41
704.617	$5s^25p^4\ ^1D_2$	$5s5p^5\ ^3P^o_1$	2.55E + 08	2.78E + 08	− 1.72	− 1.74
720.884	$5s^25p^4\ ^3P_1$	$5s5p^5\ ^3P^o_2$	1.34E + 09	1.26E + 09	− 0.99	− 1.06
721.828	$5s^25p^4\ ^1S_0$	$5s5p^5\ ^1P^o_1$	2.71E + 08	3.14E + 08	− 1.68	− 1.68
737.009	$5s^25p^4\ ^1S_0$	$5s^25p^35d\ ^5D^o_1$		2.30E + 08		− 1.80
767.520	$5s^25p^4\ ^1D_2$	$5s5p^5\ ^3P^o_2$	5.90E + 08	5.87E + 08	− 1.28	− 1.34

[a]Tauheed & Joshi (2008)
[b]Wajid & Jabeen (2019b)
[c]HFR + CPOL calculations

data set on which we can base opacity calculations of interest for modelling kilonova spectra.

4 PARTITION FUNCTIONS AND RELATIVE IONIC ABUNDANCES

Before going further into the calculation of opacities, it is useful to estimate the temperatures at which we can find the maximum abundances for the cerium ions considered, namely from Ce V to Ce X. To do this, we will place ourselves in the hypothesis of local thermodynamic equilibrium (LTE), where the Saha equation can be used. In this equation, the ionic density n_j (in cm^{-3}) corresponding to a charge state j is given by:

$$\frac{n_j}{n_{j-1}} = \frac{U_j(T)U_e(T)}{U_{j-1}(T)n_e} e^{-\chi_{j-1}/k_BT}, \tag{15}$$

where n_{j-1} is the ionic density in the j-1 charge stage, n_e is the electron density, χ_{j-1} is the ionization potential of the ion j-1, $U_j(T)$, and $U_{j-1}(T)$ are the partition functions for charge stages j and j^{-1}, respectively, computed using all the energy levels, $E_i^{(j)}$ and $E_i^{(j-1)}$, and their statistical weights, $g_i^{(j)}$ and $g_i^{(j-1)}$, belonging to the corresponding ions:

$$U_j(T) = \sum_i g_i^{(j)} e^{-E_i^{(j)}/k_BT}, \tag{16}$$

$$U_{j-1}(T) = \sum_i g_i^{(j-1)} e^{-E_i^{(j-1)}/k_BT}. \tag{17}$$

The electronic partition function, U_e, is given by:

$$U_e(T) = 2\left(\frac{m_e k_B T}{2\pi\hbar^2}\right)^{3/2}. \tag{18}$$

Using the complete set of levels calculated using the HFR + CPOL method, the number of which is given in Table 2, we evaluated

Table 6. Transition probabilities (gA) and oscillator strengths (log gf) for experimentally observed lines in Ce VIII.

λ_{obs} (Å)[a]	Transition		gA (s^{-1})		log gf	
	Lower level	Upper level	Previous[a]	This work[b]	Previous[a]	This work[b]
426.529	$5s^25p^3\ ^2D^o_{3/2}$	$5s5p^4\ ^2P_{1/2}$	2.56E + 09	2.54E + 09	− 1.15	− 1.39
440.622	$5s^25p^3\ ^4S^o_{3/2}$	$5s5p^4\ ^2S_{1/2}$	1.99E + 09	1.66E + 09	− 1.24	− 1.32
486.422	$5s^25p^3\ ^4S^o_{3/2}$	$5s5p^4\ ^2D_{5/2}$	9.96E + 07	6.56E + 07	− 2.45	− 2.64
489.149	$5s^25p^3\ ^2D^o_{3/2}$	$5s5p^4\ ^2S_{1/2}$	7.78E + 09	6.37E + 09	− 0.55	− 0.65
504.486	$5s^25p^3\ ^4S^o_{3/2}$	$5s5p^4\ ^2D_{3/2}$	1.35E + 09	1.01E + 09	− 1.29	− 1.42
546.290	$5s^25p^3\ ^2D^o_{3/2}$	$5s5p^4\ ^2D_{5/2}$	4.34E + 07	3.86E + 07	− 2.71	− 2.77
553.176	$5s^25p^3\ ^2P^o_{1/2}$	$5s5p^4\ ^2S_{1/2}$	3.70E + 09	3.24E + 09	− 0.76	− 0.84
562.502	$5s^25p^3\ ^4S^o_{3/2}$	$5s5p^4\ ^4P_{1/2}$	3.32E + 09	2.43E + 09	− 0.80	− 0.96
569.147	$5s^25p^3\ ^2D^o_{5/2}$	$5s5p^4\ ^2D_{5/2}$	1.04E + 10	8.03E + 09	− 0.29	− 0.42
569.147	$5s^25p^3\ ^2D^o_{3/2}$	$5s5p^4\ ^2D_{3/2}$	9.92E + 09	7.66E + 09	− 0.32	− 0.44
572.185	$5s^25p^3\ ^4S^o_{3/2}$	$5s5p^4\ ^4P_{3/2}$	6.48E + 09	5.00E + 09	− 0.49	− 0.63
622.891	$5s^25p^3\ ^2P^o_{3/2}$	$5s5p^4\ ^2S_{1/2}$	3.94E + 07	1.50E + 08	− 2.64	− 2.08
630.437	$5s^25p^3\ ^4S^o_{3/2}$	$5s5p^4\ ^4P_{5/2}$	4.62E + 09	3.54E + 09	− 0.55	− 0.70
644.147	$5s^25p^3\ ^2D^o_{3/2}$	$5s5p^4\ ^4P_{1/2}$	1.69E + 08	1.44E + 08	− 1.97	− 2.08
656.876	$5s^25p^3\ ^2D^o_{3/2}$	$5s5p^4\ ^4P_{3/2}$	1.52E + 06	1.79E + 06	− 4.00	− 3.96
690.223	$5s^25p^3\ ^2D^o_{5/2}$	$5s5p^4\ ^4P_{3/2}$	2.60E + 08	2.67E + 08	− 1.72	− 1.74
718.569	$5s^25p^3\ ^2P^o_{3/2}$	$5s5p^4\ ^2D_{5/2}$	2.30E + 09	2.16E + 09	− 0.74	− 0.80
734.807	$5s^25p^3\ ^2D^o_{3/2}$	$5s5p^4\ ^4P_{5/2}$	1.33E + 09	1.18E + 09	− 0.96	− 1.05
758.682	$5s^25p^3\ ^2P^o_{3/2}$	$5s5p^4\ ^2D_{3/2}$	1.97E + 07	3.84E + 06	− 2.77	− 3.51
759.920	$5s^25p^3\ ^2P^o_{1/2}$	$5s5p^4\ ^4P_{1/2}$	2.38E + 08	2.11E + 08	− 1.68	− 1.77
776.746	$5s^25p^3\ ^2D^o_{5/2}$	$5s5p^4\ ^4P_{5/2}$	5.36E + 08	5.22E + 08	− 1.30	− 1.35
777.735	$5s^25p^3\ ^2P^o_{1/2}$	$5s5p^4\ ^4P_{3/2}$	6.20E + 06	7.11E + 06	− 3.24	− 3.22
923.047	$5s^25p^3\ ^2P^o_{3/2}$	$5s5p^4\ ^4P_{3/2}$	1.12E + 08	9.41E + 07	− 1.84	− 1.97
1084.569	$5s^25p^3\ ^2P^o_{3/2}$	$5s5p^4\ ^4P_{5/2}$	1.45E + 07	1.16E + 07	− 2.58	− 2.74

[a]Wajid & Jabeen (2019a)
[b]HFR + CPOL calculations

the partition functions corresponding to Ce V to Ce X ions over a wide range of temperatures, from 1 to 100 000 K. These new partition functions, completed by those obtained for Ce I, Ce II, Ce III, and Ce IV by using the corresponding energy levels taken from the NIST database (Kramida et al. 2020) were incorporated into the Saha equation to determine the relative number of cerium atoms in different ionization stages, assuming a pure Ce gas. In these calculations, we also included the relevant ionization potentials tabulated at NIST and electron densities estimated from the mass density of the kilonova ejecta, i.e. from $\rho = 10^{-13}$ g cm^{-3} to $\rho = 10^{-10}$ g cm^{-3} when going from the first ionization degrees to higher ones, as suggested by Gaigalas et al. (2019) and Banerjee et al. (2020), respectively. This allowed us to draw the Fig. 6 representing the relative ionic cerium abundances as a function of temperature and to deduce the temperatures corresponding to the maximum abundance for each of the cerium ions considered in the present study. The values thus obtained were the following: 24 600 K for Ce V, 32 000 K for Ce VI, 39 000 K for Ce VII, 45 000 K for Ce VIII, 53 000 K for Ce IX, and 66 000 K for Ce X. It is important to note that, for the early-phases of kilonovae in which the ionization degrees V to X are supposed to be produced, a temperature of 100 000 K was systematically assumed in previous studies (Banerjee et al. 2020). In the next section, we will examine the effects of such a choice on the opacity calculations compared to the results obtained using the temperatures deduced from our work.

5 OPACITY CALCULATIONS

In a rapidly expanding environment, such as the one characterizing the ejecta from neutron star mergers, bound-bound opacities can be evaluated using the formalism of expansion opacities (see e.g. Karp et al. 1977; Eastman & Pinto 1993; Kasen, Thomas & Nugent 2006) according to which the contributions of a large number of lines to the monochromatic opacity are approximated by a discretization involving the summation of lines falling within a spectral width, while the radiative transfer is considered in the Sobolev (1960) approximation.

More precisely, in this approach, the bound-bound opacity is calculated using the expression

$$\kappa^{bb}(\lambda) = \frac{1}{\rho c t} \sum_l \frac{\lambda_l}{\Delta\lambda}(1 - e^{-\tau_l}), \tag{19}$$

where λ (in Å) is the central wavelength within the region of width $\Delta\lambda$, λ_l are the wavelengths of the lines appearing in this range, τ_l are the corresponding optical depths, c (in cm s^{-1}) is the speed of light, ρ (in g^{-1} cm^3) is the density of the ejected gas and t (in s) is the elapsed time since ejection.

The optical depth can be expressed using Sobolev (1960) formula:

$$\tau_l = \frac{\pi e^2}{m_e c} f_l n_l t \lambda_l, \tag{20}$$

where e (in C) is the elementary charge, m_e (in g) is the electron mass, f_l (dimensionless) is the oscillator strength, and n_l (in cm^{-3}) is the density of the lower level of the transition.

Let us also recall that, in this formalism, the LTE is assumed so that n_l can be expressed using the Boltzmann distribution:

$$n_l = \frac{g_l}{g_0} n e^{-E_l/k_B T}, \tag{21}$$

Table 7. Transition probabilities (gA) and oscillator strengths (log gf) for experimentally observed lines in Ce X.

λ_{obs} (Å)[a]	Transition		gA (s^{-1})		log gf	
	Lower level	Upper level	Previous[a]	This work[b]	Previous[a]	This work[b]
226.189	$5s^25p\ ^2P^o_{1/2}$	$5s^26s\ ^2S_{1/2}$	4.50E + 10	5.43E + 10		− 0.39
244.683	$5s^25p\ ^2P^o_{3/2}$	$5s^26s\ ^2S_{1/2}$	7.10E + 10	8.66E + 10		− 0.12
335.712	$5s^25p\ ^2P^o_{1/2}$	$5s^25d\ ^2D_{3/2}$	1.16E + 11	6.14E + 10		0.00
346.792	$5s5p^2\ ^4P_{3/2}$	$5s5p(^3P)5d\ ^4D^o_{5/2}$	4.20E + 10	4.48E + 10		− 0.11
348.806	$5s5p^2\ ^4P_{1/2}$	$5s5p(^3P)5d\ ^4D^o_{1/2}$	9.80E + 10	8.47E + 10		0.17
350.794	$5s5p^2\ ^4P_{1/2}$	$5s5p(^3P)5d\ ^4D^o_{3/2}$	1.16E + 11	1.05E + 11		0.27
360.090	$5s5p^2\ ^4P_{3/2}$	$5s5p(^3P)5d\ ^4D^o_{7/2}$	2.89E + 11	1.77E + 11		0.53
360.931	$5s5p^2\ ^4P_{5/2}$	$5s5p(^3P)5d\ ^4D^o_{5/2}$	8.10E + 10	8.74E + 10		0.22
372.659	$5s^25p\ ^2P^o_{3/2}$	$5s^25d\ ^2D_{5/2}$	1.93E + 11	1.77E + 11		0.55
378.142	$5s^25p\ ^2P^o_{3/2}$	$5s^25d\ ^2D_{3/2}$	2.30E + 10	2.04E + 10		− 0.38
388.513	$5s^25p\ ^2P^o_{1/2}$	$4f5s(^1F)5p\ ^2D_{3/2}$	1.00E + 10	1.07E + 10		− 0.64
408.869	$5s^25p\ ^2P^o_{1/2}$	$5s5p^2\ ^2P_{3/2}$	3.20E + 10	2.50E + 10		− 0.22
409.419	$4f5s^2\ ^2F^o_{7/2}$	$5s^25d\ ^2D_{5/2}$	7.70E + 10	7.93E + 10		0.30
411.649	$4f5s^2\ ^2F^o_{5/2}$	$5s^25d\ ^2D_{3/2}$	3.90E + 10	2.67E + 10		− 0.17
413.774	$5s^25p\ ^2P^o_{1/2}$	$5s5p^2\ ^2S_{1/2}$	3.00E + 09	3.16E + 09		− 1.10
443.372	$5s^25p\ ^2P^o_{3/2}$	$4f5s(^3F)5p\ ^2D_{5/2}$	2.30E + 10	2.06E + 10		− 0.24
446.500	$5s^25p\ ^2P^o_{3/2}$	$4f5s(^1F)5p\ ^2D_{3/2}$	7.00E + 09	4.90E + 09		− 0.86
477.297	$5s^25p\ ^2P^o_{3/2}$	$5s5p^2\ ^2P_{3/2}$	8.30E + 10	7.55E + 10		0.38
480.196	$5s^25p\ ^2P^o_{1/2}$	$5s5p^2\ ^2P_{3/2}$	4.20E + 10	3.52E + 10		0.06
480.196	$5s^25p\ ^2P^o_{3/2}$	$5s5p^2\ ^2S_{1/2}$	3.00E + 09	2.55E + 10		− 0.08
490.171	$4f5s^2\ ^2F^o_{5/2}$	$4f5s(^3F)5p\ ^2D_{5/2}$	5.00E + 09	2.91E + 09		− 0.98
493.974	$4f5s^2\ ^2F^o_{5/2}$	$4f5s(^3F)5p\ ^2D_{3/2}$	4.90E + 10	3.52E + 10		0.11
495.514	$4f5s^2\ ^2F^o_{5/2}$	$4f5s(^3F)5p\ ^2G_{7/2}$	1.15E + 11	7.51E + 10		0.44
496.427	$4f5s^2\ ^2F^o_{7/2}$	$4f5s(^3F)5p\ ^2D_{5/2}$	6.30E + 10	4.57E + 10		0.22
498.487	$4f5s^2\ ^2F^o_{7/2}$	$4f5s(^3F)5p\ ^2G_{9/2}$	1.72E + 11	1.31E + 11		0.69
501.904	$4f5s^2\ ^2F^o_{7/2}$	$4f5s(^3F)5p\ ^2G_{7/2}$	1.70E + 10	1.05E + 10		− 0.40
507.242	$4f5s^2\ ^2F^o_{5/2}$	$4f5s(^3F)5p\ ^2F_{7/2}$	1.80E + 10	1.36E + 10		− 0.28
513.167	$4f5s^2\ ^2F^o_{5/2}$	$4f5s(^3F)5p\ ^2F_{5/2}$	9.10E + 10	7.33E + 10		0.46
513.948	$4f5s^2\ ^2F^o_{7/2}$	$4f5s(^3F)5p\ ^2F_{7/2}$	1.12E + 11	8.98E + 10		0.55
519.115	$5s^25p\ ^2P^o_{1/2}$	$5s5p^2\ ^2D_{3/2}$	1.40E + 10	6.96E + 09		− 0.54
572.011	$5s^25p\ ^2P^o_{3/2}$	$5s5p^2\ ^2P_{1/2}$	2.00E + 09	1.09E + 09		− 1.30
578.268	$5s^25p\ ^2P^o_{3/2}$	$5s5p^2\ ^2D_{5/2}$	7.00E + 09	3.95E + 09		− 0.69
717.173	$5s^25p\ ^2P^o_{1/2}$	$5s5p^2\ ^4P_{1/2}$	1.00E + 09	4.42E + 08		− 1.45
732.436	$5s^25p\ ^2P^o_{3/2}$	$5s5p^2\ ^4P_{5/2}$	2.00E + 09	1.44E + 09		− 0.92

[a]Joshi et al. (2001)
[b]HFR + CPOL calculations

where k_B is the Boltzmann constant (in $cm^{-1}\,K^{-1}$), T (in K) is the temperature, g_l and E_l (in cm^{-1}) are respectively the statistical weight and the energy of the lower level of the transition, and g_0 is the statistical weight of the ground level for the ion considered.

We can then write the optical depth as

$$\tau_l = \frac{\pi e^2}{m_e c}\left(\frac{n\lambda_l t}{g_0}\right) g_l f_l e^{-E_l/k_B T}. \quad (22)$$

The astrophysical opacities were then calculated using the expressions mentioned above for Ce V – X ions with the refined temperatures obtained in Section 4, namely $T = 24\,600$ K (Ce V), 32 000 K (Ce VI), 39 000 K (Ce VII), 45 000 K (Ce VIII), 53 000 K (Ce IX), and 66 000 K (Ce X). The density was fixed at $\rho = 10^{-10}$ g . cm^{-3} and the time after merger was $t = 0.1$ d, as suggested by Banerjee et al. (2020) for the early phases of kilonovae in which such ionization stages are expected to be present. Moreover, we used $\Delta\lambda = 5$ Å, according to our previous similar work in Ce II, Ce III, and Ce IV ions (Carvajal Gallego et al. 2021).

For each Ce ion considered in the present work, the radiative data obtained with the HFR + CPOL method were included in opacity calculations, considering all transitions involving energy levels below the relevant ionization potentials and for which the computed log gf-values were found to be greater than −5.0. This limit was chosen because weaker transitions appeared to have negligible contributions to the opacities, as shown in Fig. 7 where the opacities calculated for the Ce VI ion using the transitions with log $gf > -2$, log $gf > -5$, and log $gf > -6$ are compared. From this figure, it can be clearly observed that the difference between the last two curves is minimal, thus showing a convergence of the results for log $gf > -5$ and therefore that it is not necessary to include transitions with smaller oscillator strengths in the opacity calculations. It should be noted that this convergence of expansion opacities was also obtained by Fontes et al. (2020) who showed in Fig. 11 of their paper that the opacities no longer varied when including transitions with log $gf < -5$, in the case of neutral neodymium.

For each cerium ionic charge state, the final number of lines, as well as the ionization potential used for computing bound-bound opacities, are given in Table 9. Note that many transitions were included in the calculations, ranging from a hundred thousand lines (for Ce X) to over one million (for Ce VIII). The opacities thus obtained are plotted versus wavelengths in Figs 8, 9, 10, 11, 12, and 13 for Ce V, Ce VI, Ce VII, Ce VIII, Ce IX, and Ce X, respectively.

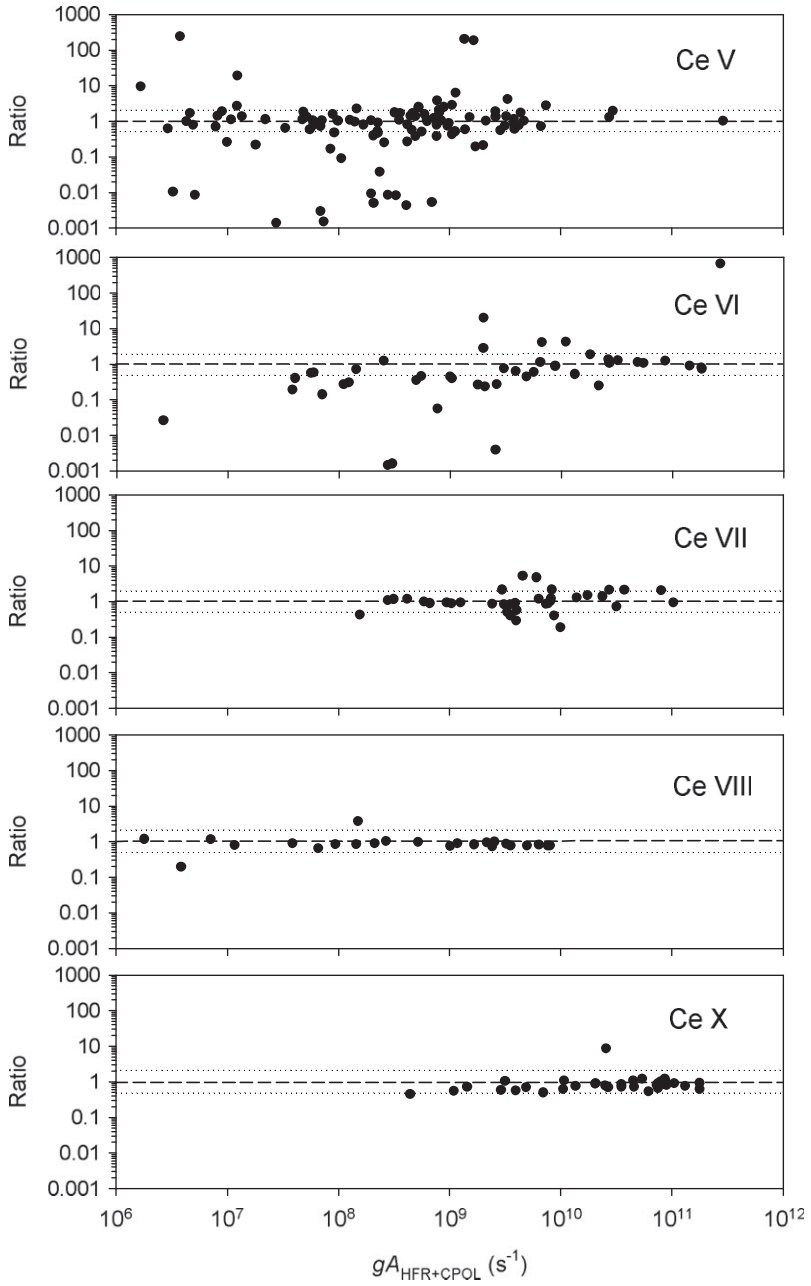

Figure 3. Comparison between HFR + CPOL transition probabilities (gA) and previously published values for experimentally observed lines in Ce V, Ce VI, Ce VII, Ce VIII ,and Ce X ions. For each ion, the ratio $gA_{HFR+CPOL}$ / $gA_{Previous}$ is plotted against $gA_{HFR+CPOL}$. The dashed lines correspond to ratios equal to unity while the dotted lines correspond to deviations of a factor of two.

Looking at these figures, we see that the expansion opacity varies roughly between 0.01 and 40 $cm^2\ g^{-1}$, depending on the ionic charge, the maximum of opacity being always located at UV wavelengths around 500 Å. Interesting is the comparison we can make with the opacities calculated under similar conditions of kilonova early phases (i.e. for $T = 100\,000$ K, $\rho = 10^{-10}$ g cm^{-3}, and $t = 0.1$ d) by Banerjee et al. (2020) who considered only elements lighter than the lanthanides, namely those between $Z = 20$ (Ca) and $Z = 56$ (Ba). We note that their opacities vary between 0.001 and 4 $cm^2\ g^{-1}$, i.e. one order of magnitude smaller than those obtained in our work for cerium ions, thus confirming the preponderance of the contribution of lanthanides (whatever their ionization degree) to the opacity characterizing the kilonova spectra.

Finally, the influence of the choice of temperature on the opacities was estimated. In particular, we compared the opacities computed using the temperatures that we deduced from the relative ionic abundance analysis described in Section 4 with the results obtained using the temperature usually considered in previous works for V – X ions, namely $T = 100\,000$ K (Banerjee et al. 2020). From this analysis, it appeared that the choice of the temperature is not trivial in so far as the opacities seem to be effectively affected by this choice. This is illustrated in Fig. 14 in which the opacities obtained for Ce VIII using our refined temperature ($T = 45\,000$ K) are compared with those calculated with $T = 100\,000$ K. A deviation of about one order of magnitude can be seen (especially for long wavelengths), the values obtained with $T = 100\,000$ K appearing systematically larger

Table 8. Comparison between oscillator strengths (log *gf*) obtained in the present work using HFR + CPOL, MCDHF, and AMBiT methods for a sample of lines in Ce V, Ce VIII, and Ce X.

λ_{obs} (Å)[a]	log *gf*		
	HFR + CPOL	MCDHF	AMBiT
Ce V			
399.361	0.76	0.75	0.81
482.963	− 0.70	− 0.43	− 0.53
552.134	− 2.64	− 2.41	− 2.52
936.241	− 1.58	− 1.01	− 1.19
1141.824	− 2.57	− 2.51	− 2.48
1186.865	− 1.98	− 1.85	− 1.94
1205.859	− 1.54	− 1.41	− 1.47
1211.818	− 1.29	− 1.03	− 1.15
1234.403	− 2.28	− 2.18	− 2.15
1250.718	− 3.70	− 3.65	− 5.58
1264.429	− 2.57	− 2.42	− 2.50
1286.305	− 2.10	− 2.04	− 2.12
1299.297	− 0.72	− 0.56	− 0.64
1309.589	− 2.68	− 2.55	− 2.30
1315.354	− 1.41	− 1.30	− 1.35
1315.826	− 0.77	− 0.60	− 0.68
1331.550	− 4.00	− 0.69	− 0.76
1341.640	− 0.77	− 0.66	− 0.71
1356.192	− 1.54	− 1.42	− 1.47
1358.358	− 0.84	− 0.75	− 0.81
1360.331	− 1.85	− 1.73	− 1.76
1360.786	− 2.96	− 3.45	− 2.95
1362.125	− 0.61	− 0.51	− 0.55
1362.668	− 0.88	− 0.78	− 0.85
1365.964	− 1.75	− 1.70	− 1.73
1385.346	− 2.42	− 2.87	− 2.18
1401.064	− 0.96	− 0.82	− 0.88
1409.195	− 1.51	− 1.39	− 1.44
1414.959	− 1.21	− 1.08	− 1.13
1423.824	− 1.63	− 1.50	− 1.52
1444.901	− 2.77	− 2.76	− 2.80
1494.356	− 1.64	− 1.52	− 1.58
1508.812	− 2.34	− 2.52	− 2.56
1532.497	− 1.57	− 1.45	− 1.50
1568.225	− 2.48	− 2.55	− 2.43
1575.641	− 1.46	− 1.51	− 1.52
1741.233	− 2.68	− 2.49	− 2.56
1765.111	− 2.35	− 2.40	− 2.33
1767.382	− 3.52	− 3.68	− 3.37
1841.673	− 5.00	− 3.92	− 3.16
1955.172	− 3.30	− 3.13	− 3.00
2095.999	− 2.66	− 2.49	− 2.51
2141.969	− 2.39	− 2.49	− 2.29
2178.222	− 2.57	− 2.45	− 2.41
Ce VIII			
440.622	− 1.32	− 2.83	− 1.31
486.422	− 2.64	− 2.31	− 2.51
489.149	− 0.65	− 0.48	− 0.65
504.486	− 1.42	− 1.21	− 1.23
546.290	− 2.77	− 2.51	− 2.63
553.176	− 0.84	− 0.67	− 0.85
562.502	− 0.96	− 0.75	− 0.78
569.147	− 0.42	− 0.22	− 0.27
569.147	− 0.44	− 0.23	− 0.29
572.185	− 0.63	− 0.41	− 0.47
622.891	− 2.08	− 1.83	− 2.57
630.437	− 0.70	− 0.51	− 0.54
644.147	− 2.08	− 2.04	− 1.94
656.876	− 3.96	− 2.94	− 4.12
690.223	− 1.74	− 1.49	− 1.69
718.569	− 0.80	− 0.68	− 0.71
734.807	− 1.05	− 0.93	− 0.94
758.682	− 3.51	− 6.18	− 2.82
759.920	− 1.77	− 1.57	− 1.66
776.746	− 1.35	− 1.21	− 1.27
777.735	− 3.22	− 3.29	− 3.15
923.047	− 1.97	− 1.93	− 1.82
1084.569	− 2.74	− 2.79	− 2.62
Ce X			
335.712	0.00	0.01	0.20
346.792	− 0.11	− 0.01	− 0.07
348.806	0.17	0.13	0.19
350.794	0.27	− 0.11	0.07
360.090	0.53	0.67	0.55
360.931	0.22	0.22	0.19
372.659	0.55	0.41	− 0.02
378.142	− 0.38	− 0.56	− 0.32
388.513	− 0.64	− 0.73	− 0.40
408.869	− 0.22	− 0.36	− 0.08
409.419	0.30	0.13	0.26
411.649	− 0.17	− 0.19	0.12
413.774	− 1.10	− 1.50	− 0.84
443.372	− 0.24	− 0.30	− 0.02
446.500	− 0.86	− 0.93	− 0.57
477.297	0.38	0.21	0.48
480.196	0.06	0.06	0.17
480.196	− 0.08	− 0.12	0.05
490.171	− 0.98	− 2.11	− 0.67
493.974	0.11	0.07	0.14
495.514	0.44	0.52	0.64
496.427	0.22	0.20	0.26
498.487	0.69	0.69	0.80
501.904	− 0.40	− 0.38	− 0.28
507.242	− 0.28	− 0.33	− 0.25
513.167	0.46	0.39	0.56
513.948	0.55	0.50	0.67
519.115	− 0.54	− 0.33	− 0.18
572.011	− 1.30	− 1.02	− 1.49
578.268	− 0.69	− 0.58	− 0.46
717.173	− 1.45	− 1.27	− 1.34
732.436	− 0.92	− 0.78	− 0.83

[a]Extracted from Tables 3, 6, and 7 for Ce V, Ce VIII, and Ce X, respectively.

than those obtained with our refined temperature. The decrease in opacity with wavelength is also more marked with our temperature value than with $T = 100\,000$ K.

6 CONCLUSION

Extensive atomic structure calculations were performed in order to obtain a large amount of radiative parameters for moderately charged cerium ions between Ce V and Ce X. For this purpose, three independent theoretical approaches were used, namely the HFR + CPOL, MCDHF, and AMBiT methods. From detailed comparisons between the results obtained by these three methods, as well as from comparisons between our data with the few previously published experimental and theoretical investigations, it was possible to determine a reliable set of theoretical wavelengths, transition

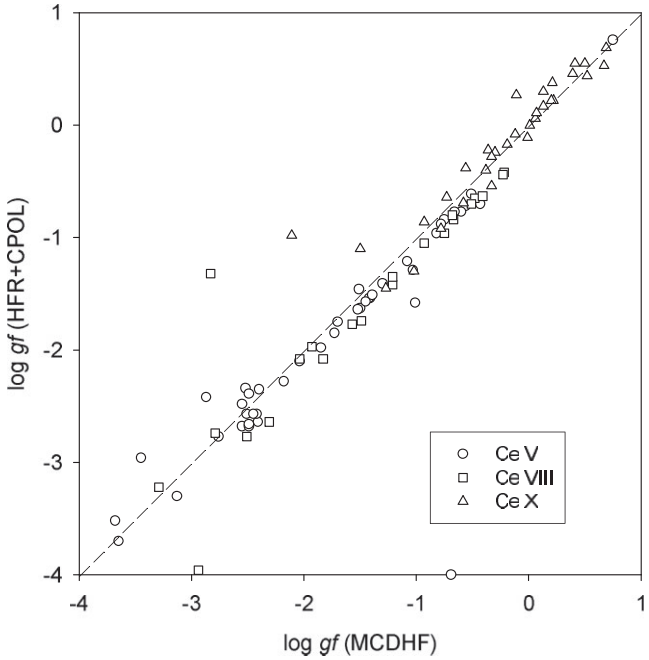

Figure 4. Comparison between oscillator strengths (log *gf*) computed in the present work using the HFR + CPOL and MCDHF methods for experimentally observed lines in Ce V, Ce VIII, and Ce X ions.

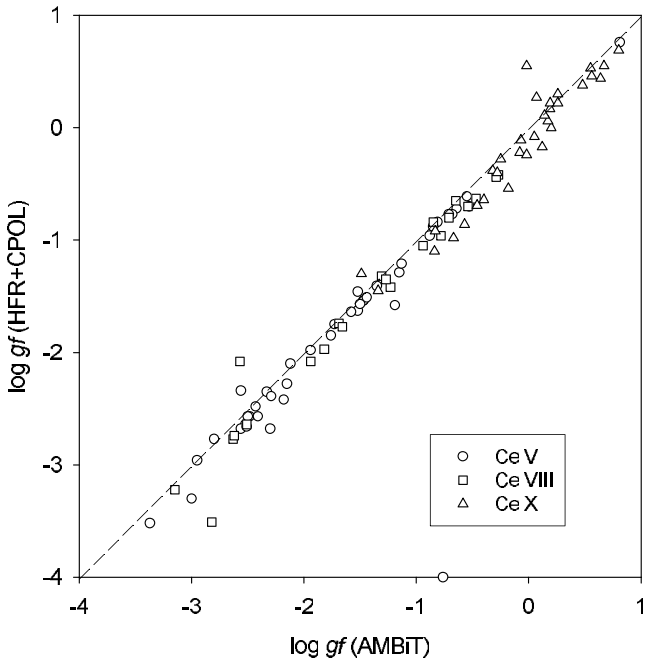

Figure 5. Comparison between oscillator strengths (log *gf*) computed in the present work using the HFR + CPOL and AMBiT methods for experimentally observed lines in Ce V, Ce VIII, and Ce X ions.

probabilities, and oscillator strengths for a very large number of spectral lines (nearly 4 million in total) in these six Ce ions.

All the new HFR + CPOL atomic data (validated by the good agreement observed with the MCDHF and AMBiT results in many cases) were then used to calculate the monochromatic opacities for the spectral study of the early phases of kilonovae observed after neutron star mergers, i.e. for typical kilonova conditions such as T

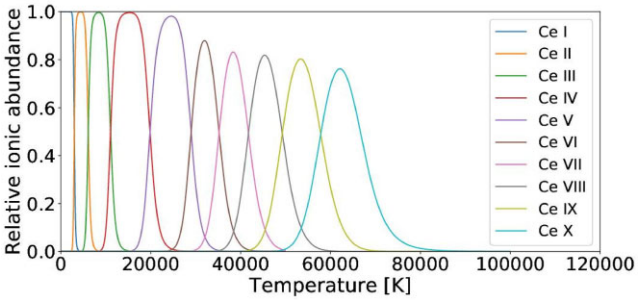

Figure 6. Relative ionic abundances for Ce I–X species as a function of temperature.

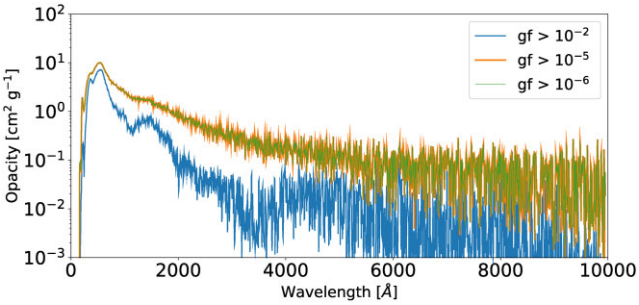

Figure 7. Comparison between bound-bound opacities calculated in the case of Ce VI using transitions with HFR + CPOL oscillator strengths such as log $gf > -2$, log $gf > -5$, and log $gf > -6$.

Table 9. Ionization potentials and numbers of spectral lines included in the opacity calculations for Ce V – X ions.

Ion	IP (cm^{-1})[a]	Number of lines[b]
Ce V	528 700	131 248
Ce VI	626 000	657 090
Ce VII	734 000	918 542
Ce VIII	855 000	1113 548
Ce IX	1008 000	834 383
Ce X	1129 000	99 259

[a]From NIST atomic database (Kramida et al. 2020)
[b]Number of transitions involving energy levels below the IP with HFR + CPOL calculated log *gf*-values greater than 5 (see text)

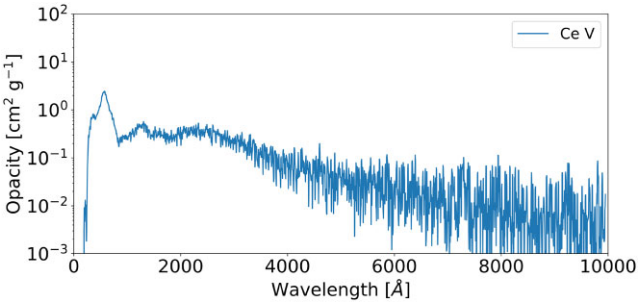

Figure 8. Expansion opacity for Ce V, calculated with $T = 24\,600$ K, $\rho = 10^{-10}$ g cm^{-3}, $t = 0.1$ d, and $\Delta\lambda = 5$ Å.

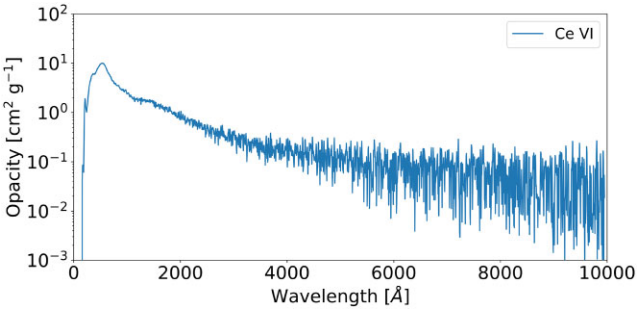

Figure 9. Expansion opacity for Ce VI, calculated with $T = 32\,000$ K, $\rho = 10^{-10}$ g cm^{-3}, $t = 0.1$ d, and $\Delta\lambda = 5$ Å.

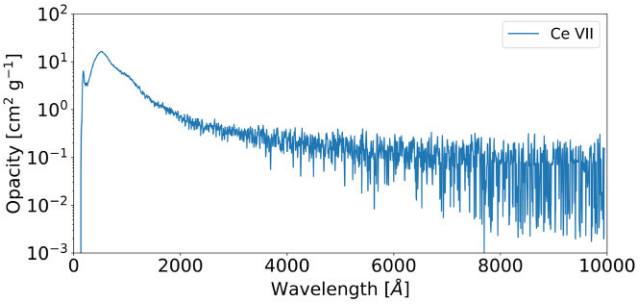

Figure 10. Expansion opacity for Ce VII, calculated with $T = 39\,000$ K, $\rho = 10^{-10}$ g cm^{-3}, $t = 0.1$ d, and $\Delta\lambda = 5$ Å.

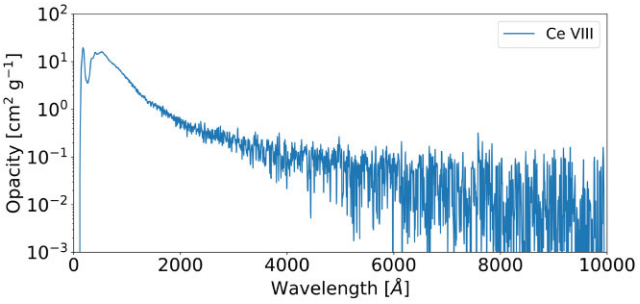

Figure 11. Expansion opacity for Ce VIII, calculated with $T = 45\,000$ K, $\rho = 10^{-10}$ g cm^{-3}, $t = 0.1$ d, and $\Delta\lambda = 5$ Å.

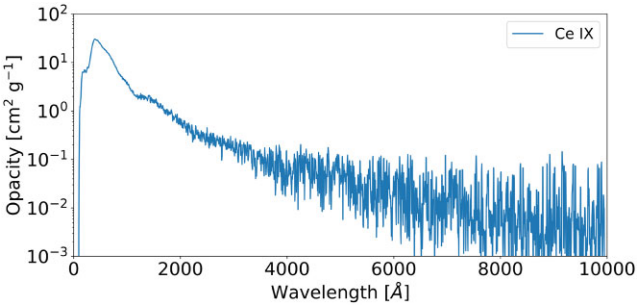

Figure 12. Expansion opacity for Ce IX, calculated with $T = 53\,000$ K, $\rho = 10^{-10}$ g cm^{-3}, $t = 0.1$ d, and $\Delta\lambda = 5$ Å.

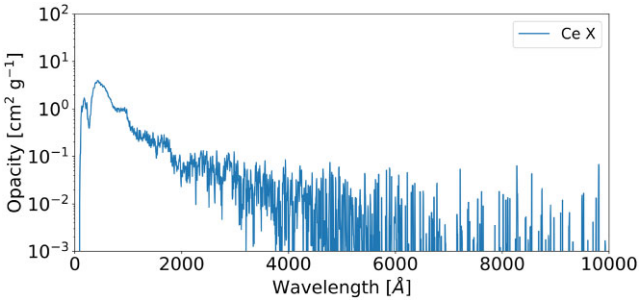

Figure 13. Expansion opacity for Ce X, calculated with $T = 66\,000$ K, $\rho = 10^{-10}$ g cm^{-3}, $t = 0.1$ d, and $\Delta\lambda = 5$ Å.

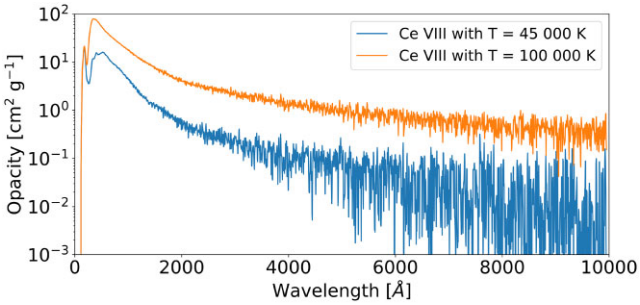

Figure 14. Comparison between the opacities calculated for Ce VIII using $T = 45\,000$ K and $T = 100\,000$ K.

$> 20\,000$ K, $\rho = 10^{-10}$ g . cm^{-3} and $t = 0.1$ d. On the basis of the numerous energy levels computed in the present work, we were able to calculate precise partition functions and to deduce, by using the Saha equation, refined temperatures corresponding to the ionic abundance maxima for Ce V – X ions. This allowed us to show that the use of these temperatures, instead of the one usually used for the early phases of kilonovae, i.e. $T = 100\,000$ K, had a non-negligible influence on the opacity calculations.

The results reported in this paper represent the first complete and consistent set of reliable atomic data in Ce V – X ions and lay the groundwork for similar studies we plan to perform in the near future for other moderately charged lanthanide atoms of interest for the analysis of kilonova spectra.

ACKNOWLEDGEMENTS

HCG is a holder of a FRIA fellowship, while PP and PQ are, respectively, Research Associate and Research Director of the Belgian Fund for Scientific Research F.R.S.-FNRS. Financial support from these organizations is gratefully acknowledged. Computational resources have been provided by the Consortium des Equipements de Calcul Intensif (CECI), funded by the F.R.S. -FNRS under grant no. 2.5020.11 and by the Walloon Region of Belgium.

DATA AVAILABILITY

The data underlying this article will be shared on reasonable request to the corresponding author.

REFERENCES

Abbott B. P. et al., 2017a, Phys. Rev. Lett., 119, 161101
Abbott B. P. et al., 2017b, ApJ, 848, L13

Banerjee S., Tanaka M., Kawaguchi K., Kato D., Gaigalas G., 2020, ApJS, 901, 29
Bar Shalom A., Klapisch M., Oreg J., 2001, J. Quant. Spectrosc. Radiat. Transf., 71, 169
Berengut J. C., 2016, Phys. Rev. A, 94, 012502
Carvajal Gallego H., Palmeri P., Quinet P., 2021, MNRAS, 501, 1440
Churilov S. S., Joshi Y. N., 2000, J. Opt. Soc. Am. B, 17, 2081
Cowan R. D., 1981, The Theory of Atomic Structure and Spectra. California Univ. Press, Berkeley
Eastman R. G., Pinto P. A., 1993, ApJ, 412, 731
Fontes C. J., Fryer C. L., Hungerford A. L., Wollaeger R. T., Korobkin O., 2020, MNRAS, 493, 4143
Fraga S., Karwowski J., Saxena K. M. S., 1976, Handbook of Atomic Data. Elsevier, Amsterdam
Froese Fischer C., Godefroid M., Brage T., Jönsson P., Gaigalas G., 2016, J. Phys. B: At. Mol. Opt. Phys., 49, 182004
Froese Fischer C., Gaigalas G., Jönsson J. B., 2019, Comput. Phys. Commun., 237, 184
Gaigalas G., Kato D., Rynkun P., Radžiūtė L., Tanaka M., 2019, ApJS, 240, 29
Gaigalas G., Rynkun P., Radžiūtė L., Kato D., Tanaka M., Jönsson P., 2020, ApJS, 248, 13
Geddes A. J., Czapski D. A., Kahl E. V., Berengut J. C., 2018, Phys. Rev. A, 98, 042508
Grant I. P., 2007, Relativistic Quantum Theory of Atoms and Molecules. Springer, New York
Hameed S., 1972, J. Phys. B, 5, 746
Hameed S., Herzenberg A., James M. G., 1968, J. Phys. B, 1, 822
Joshi Y. N., Ryabtsev A. N., Churilov S. S., 2001, Phys. Scr., 64, 326
Kahl E. V., Berengut J. C., 2019, Comput. Phys. Commun., 238, 232
Karp H., Lasher G., Chan K. L., Salpeter E. E., 1977, ApJ, 214, 161
Kasen D., Thomas R. C., Nugent P., 2006, ApJ, 651, 366
Kasen D., Metzger B., Barnes J., Quataert E., Ramirez-Ruiz E., 2017, Nature, 551, 80
Kramida A., Ralchenko Yu., Reader J., NIST ASD Team, 2020, NIST Atomic Spectra Database (ver.5.7.1.), Available online at https://physics.nist.gov/asd (accessed in September 2021)
Kühn S. et al., 2020, Phys. Rev. Lett., 124, 225001
Quinet P., 2017, Can. J. Phys., 95, 790
Quinet P., Palmeri P., 2020, Atoms, 8, 18
Quinet P., Palmeri P., Biémont E., McCurdy M. M., Rieger G., Pinnington E. H., Wickliffe M. E., Lawler J. E., 1999, MNRAS, 307, 934
Quinet P., Palmeri P., Biémont E., Li Z. S., Zhang Z. G., Svanberg S., 2002, J. Alloys Comp., 344, 255
Radžiūtė L., Gaigalas G., Kato D., Rynkun P., Tanaka M., 2020, ApJS, 248, 17
Sobolev V. V., 1960, Moving Envelopes of Stars. Harvard University Press, Cambridge
Tanaka M. et al., 2018, ApJ, 852, 109
Tanaka M., Kato D., Gaigalas G., Kawaguchi K., 2020, MNRAS, 496, 1369
Tauheed A., Joshi Y. N., 2008, Can. J. Phys., 86, 714
Wajid A., Jabeen S., 2019a, J. At. Mol. Condens. Nano Phys., 6, 53
Wajid A., Jabeen S., 2019b, J. At. Mol. Condens. Nano Phys., 6, 123
Wajid A., Tauheed A., Jabeen S., 2021, J. Quant. Spectrosc. Rad. Transf., 258, 107387

This paper has been typeset from a TEX/LATEX file prepared by the author.